

AD-A157 666

OXIDE CATHODE MECHANISMS: ELECTRONIC AND STRUCTURAL

1/1

FEATURES OF OXIDE CAT. (U) UNIVERSITY COLL CORK

(IRELAND) DEPT OF CHEMISTRY J CUNNINGHAM ET AL. JAN 85

UNCLASSIFIED

AFMNL-TR-84-4158 AFOSR-83-0074

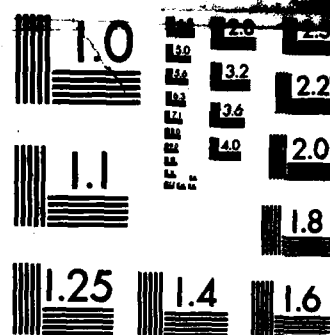
F/G 9/1

NL

END

FILMED

DTIC



MICROCOPY RESOLUTION TEST CHART
NATIONAL BUREAU OF STANDARDS-1963-A

AFWAL-TR-84-4158

AD-A157 666



**OXIDE CATHODE MECHANISMS: ELECTRONIC AND STRUCTURAL FEATURES
OF OXIDE CATHODE SURFACES**

**Professor Joseph Cunningham
Dr. John Nunan**

**Chemistry Department
University College Cork
Cork, Ireland**

January 1985

Final Report for Period 1 March 1983 - 29 February 1984

Approved for public release; distribution unlimited.

DTIC FILE COPY

**MATERIALS LABORATORY
AIR FORCE WRIGHT AERONAUTICAL LABORATORIES
AIR FORCE SYSTEMS COMMAND
WRIGHT-PATTERSON AIR FORCE BASE, OHIO 45433**



85 7 23 037

NOTICE

When Government drawings, specifications, or other data are used for any purpose other than in connection with a definitely related Government procurement operation, the United States Government thereby incurs no responsibility nor any obligation whatsoever; and the fact that the government may have formulated, furnished, or in any way supplied the said drawings, specifications, or other data, is not to be regarded by implication or otherwise as in any manner licensing the holder or any other person or corporation, or conveying any rights or permission to manufacture use, or sell any patented invention that may in any way be related thereto.

This report has been reviewed by the Office of Public Affairs (ASD/PA) and is releasable to the National Technical Information Service (NTIS). At NTIS, it will be available to the general public, including foreign nations.

This technical report has been reviewed and is approved for publication.

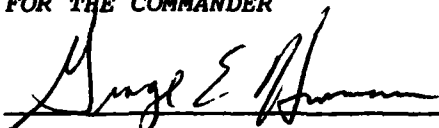


T. W. HAAS
Project Engineer
Mechanics & Surface Interactions Br



S. W. TSAI, Chief
Mechanics & Surface Interactions Br
Nonmetallic Materials Division

FOR THE COMMANDER



GEORGE E. HUSMAN, Chief
Nonmetallic Materials Division

If your address has changed, if you wish to be removed from our mailing list, or if the addressee is no longer employed by your organization please notify AFWAL/MLEM, W-PAFB, OH 45433 to help us maintain a current mailing list.

Copies of this report should not be returned unless return is required by security considerations, contractual obligations, or notice on a specific document.

Unclassified

SECURITY CLASSIFICATION OF THIS PAGE

AD A157 666

REPORT DOCUMENTATION PAGE

1a. REPORT SECURITY CLASSIFICATION Unclassified			1b. RESTRICTIVE MARKINGS	
2a. SECURITY CLASSIFICATION AUTHORITY			3. DISTRIBUTION/AVAILABILITY OF REPORT Approved for public release; distribution unlimited.	
2b. DECLASSIFICATION/DOWNGRADING SCHEDULE				
4. PERFORMING ORGANIZATION REPORT NUMBER(S)			5. MONITORING ORGANIZATION REPORT NUMBER(S) AFWAL-TR-84-4158	
6a. NAME OF PERFORMING ORGANIZATION Chemistry Department University College Cork		6b. OFFICE SYMBOL (If applicable)	7a. NAME OF MONITORING ORGANIZATION AFWAL/MLEM	
6c. ADDRESS (City, State and ZIP Code) Cork Ireland			7b. ADDRESS (City, State and ZIP Code) Wright-Patterson Air Force Base, Ohio 45433	
8a. NAME OF FUNDING/SPONSORING ORGANIZATION EOARD		8b. OFFICE SYMBOL (If applicable)	9. PROCUREMENT INSTRUMENT IDENTIFICATION NUMBER AFOSR-83-0074	
8c. ADDRESS (City, State and ZIP Code) 223 Old Marylebone Road London NW1 5TH			10. SOURCE OF FUNDING NOS.	
			PROGRAM ELEMENT NO. 62102F	PROJECT NO. 2423
11. TITLE (Include Security Classification) OXIDE CATHODE MECHANISMS: Electronic (Cont)				
12. PERSONAL AUTHOR(S) Joseph Cunningham				
13a. TYPE OF REPORT Final		13b. TIME COVERED FROM 1 Mar 83 TO 29 Feb 84		14. DATE OF REPORT (Yr., Mo., Day) January 1985
15. PAGE COUNT 72				
16. SUPPLEMENTARY NOTATION Following presentation of parts of the enclosed results at relevant scientific conferences in Europe, publication in Conference Proceedings/scientific journals shall ensue as follows: (i) in book form by Elsevier under the title "Adsorption and (Cont)				
17. COSATI CODES			18. SUBJECT TERMS (Continue on reverse if necessary and identify by block number)	
FIELD	GROUP	SUB. GR.	Oxide Cathode Materials Reconstruction of Ba ²⁺ -Doped	
			Oxide Cathode Surfaces Oxide Surfaces	
			Luminescence from Oxide Surfaces	
19. ABSTRACT (Continue on reverse if necessary and identify by block number)				
Continued from Blk 11: and Structural Features of Oxide Cathode Surfaces.				
Continued from Blk 16: Catalysis on Oxide Surfaces"; (ii) in JCS Faraday Transaction I as two scientific papers.				
ABSTRACT: The experiments and computations described in this report were directed towards (A) improved understanding of the influence of monolayer coatings of Ba ⁰ upon the work function of BaO and SrO layers prepared in UHV, and (B) more precise characterization of surface-structure and surface-reactivity features of polycrystalline mixed-oxide supports prepared in similar fashion to those incorporated in 'oxide cathode' devices. In respect of objective (A), results are presented for the changes in work function, $\Delta\phi$, and those in AES and UPS				
(Continued)				
20. DISTRIBUTION/AVAILABILITY OF ABSTRACT UNCLASSIFIED/UNLIMITED <input checked="" type="checkbox"/> SAME AS RPT. <input type="checkbox"/> DTIC USERS <input type="checkbox"/>			21. ABSTRACT SECURITY CLASSIFICATION Unclassified	
22a. NAME OF RESPONSIBLE INDIVIDUAL T. Haas			22b. TELEPHONE NUMBER (Include Area Code) 513-255-5892	22c. OFFICE SYMBOL AFWAL/MLEM

spectra caused by the controlled deposition of barium metal at submonolayer and higher coverages, θ_{Ba} , onto clean polycrystalline layers of SrO and BaO. In efforts to model selected features of oxide cathodes, the oxide layers were themselves prepared on a clean nickel support by evaporation and subsequent oxidation of multilayer deposits of strontium metal (to ultimately yield SrO) or of barium metal (to ultimately yield BaO). Plots of $\Delta\phi$ vs. θ_{Ba} confirm the expected decline in work function with θ_{Ba} up to values of the latter ca. 0.5 monolayer. Quantitatively the profile of these Ba²⁺-induced changes in work function for freshly prepared layers of SrO or BaO did not differ markedly from " $\Delta\phi$ vs. θ_{Ba} " profile reported for barium as evaporated layers on metals such as tungsten. Such results thus emphasized the role of θ_{Ba} but did not reveal features associated with the surface structure oxide support.

Possibilities for significant influence of the surface structure of 'mixed oxide' supports upon electronic energy levels of surface states and for the occurrence of surface sites favouring low work function, emerge clearly from our studies of polycrystalline BaO/MgO, BaO/CaO and BaO/SrO systems. Studies of the surface properties of these systems, - made using surface luminescence to probe electronic energy levels and gaseous molecules to examine surface reactivity, - are shown to be consistent with a hitherto unrecognised reconstruction ('rumpling') of the mixed oxide surfaces caused by segregation of Ba²⁺ to the surface. Theoretical support for such segregation and surface reconstruction has furthermore come from recent computations by other workers, thus pointing to the need to take these into account for meaningful progress towards objective (B) above. In respect of present surface-luminescence studies it appears that this technique offers a valuable non-destructive probe for such reconstruction, and points to its establishment by prior thermal activation in vacuo at 900-1173 K. (These observations are reminiscent of 'activity vs. preactivation' behaviour of oxide cathodes).

The molecular gas conversions employed to examine reactivity of the Ba²⁺-doped surfaces at 300 K (i.e. in conditions approximating those of an oxide cathode in its non-operating states) were $N_2O \xrightarrow{Ba^{2+}} N_2 + O(ads)$ and $^{16}O_2 + ^{18}O_2 \xrightarrow{Ba^{2+}} 2^{16}O^{18}O$. Comparisons of the reactivity of Ba²⁺-doped and pure oxides reveal enhanced activity consistent with an identification of active sites as (i) having Ba²⁺ displaced outward in the surface reconstruction to positions of high coordinative unsaturation (cus) and (ii) having excess electrons localised in the proximity of Ba^{cus}. At temperatures approaching those used in the 'working state' of oxide cathodes, only the $N_2O \rightarrow N_2 + \frac{1}{2}O_2$ conversion was found useful for monitoring greatly enhanced activity and its dependence upon level of loading of the surfaces by Ba²⁺.

PREFACE

The work described on this report originated from an interest - shared by the Principal Investigator with AFOSR scientists at EOARD and at AFWAL - in reassessing the surface-electronic and surface-defect properties of the polycrystalline alkaline earth oxides on which Oxide cathodes are based.

Dr. T.W. Haas at AFWAL/MLBM, Wright Patterson AFB was Program Manager throughout both phases of the work: Phase One, from 1 October, 1981 to 30 September, 1982, sponsored by EOARD and funded under Grant No. AFOSR-82-0023; and Phase Two, from 1 March, 1983 to 29 February, 1984, sponsored by AFWAL and funded under Grant No. AFOSR 83-0074.

Professor J. Cunningham at University College Cork was Principal Investigator throughout both phases of the project. Novel features of the project were the design of model systems which modelled various aspects of Oxide Cathodes and the application to these systems of techniques not previously utilised to assess surface-defect and surface-electronic properties of Oxide Cathodes. Dr. John Nunan, who was funded as a Postdoctoral Research Associate throughout the project, was involved in all experimental aspects of the project. The work has already resulted in submission of three papers to scientific journals.

(iii)

[illegible]

CONTENTS

	LIST OF ILLUSTRATIONS	(v)
I	INTRODUCTION	1
II	SUMMARY - RESULTS AND CONCLUSIONS	4
	APPENDIX A : SURFACE PROCESSES ON STRONTIUM OXIDE PREACTIVATED AT VARIOUS TEMPERATURES	12
	APPENDIX B : EFFECTS OF Ba^{2+} DOPANT UPON SURFACE PROCESSES ON MgO	50
	APPENDIX C : EFFECTS OF SUBMONOLAYER COVERAGES BY ZERO VALENT Ba^0 UPON WORK FUNCTION OF LAYERS OF SrO OR BaO PREPARED IN UHV.	72

PREVIOUS PAGE
IS BLANK

LIST OF ILLUSTRATIONS

- FIG. 1: Difference Excitation Spectra for BaO/MgO, Plot (A), BaO/CaO, Plot (B) and BaO/SrO, Plot (C). All samples at loading >3 m.e.
(page 6)
- FIG. 2: Variation of Relative Intensities of Ba²⁺-related Emission with $\lambda_{(\text{max})} = 460 \text{ nm}$ from Ba²⁺/MgO samples having the Indicated Nominal Surface Loadings (monolayer equivalents) of Ba²⁺ ($\lambda_{\text{ex}} = 335 \text{ nm}$).
(page 6)
- FIG. A-1a&b: Study of SrCO₃ Decomposition as a Function of Outgassing Temperature
(page 21)
A = CO + CO₂ composition in gas phase above the sample
B = Total pressure of decomposition products over the sample.
- FIG. A-1c: Plot of CO/CO₂ Ratio in the Decomposition Product as a Function of Outgassing Temperature for SrCO₃.
(page 22)
- FIG. A-2a&b: Excitation Spectra (Fig. A-2a) and Emission Spectra (Fig. A-2b) of SrO (ex SrCO₃) outgassed at Various Temperatures between 1073 K and 1293 K: A(i) and B(i) Excitation and Emission Spectra respectively from SrO outgassing for one hour at 1073 K; A(ii) and B(ii) Spectra after outgassing for one hour at 1123 K; A(iii) and B(iii) spectra after outgassing at 1123 K for one hour; A(iv) and B(iv) spectra after outgassing at 1173/1273 K for one hour; A(v) and B(v) spectra after outgassing at 1293 K for four hours.
(page 24)
- FIG. A-3a&b: Emission Spectra of SrCO₃ excited by different wavelengths of Exciting Light after outgassing at 1073 (Fig. 3A) and 1293 K (Fig. 3B): Plots A(i) and B(i) are emission spectra observed under excitation at $\lambda = 280 \text{ nm}$ from SrO outgassed at 1073 and 1273 K respectively; A(ii) and B(ii) emission spectra excited at $\lambda = 299 \text{ nm}$ from SrO outgassed at 1073 and 1273 K respectively; A(iii) and B(iii) emission spectra excited at $\lambda = 315 \text{ nm}$ from SrO outgassed at 1073 and 1293 K respectively; B(iv) emission spectra excited at $\lambda = 325 \text{ nm}$ from SrO outgassed for one hour at 1173/1293 K.
(page 25)

- FIG. A-4: First Order Plots for N_2O Decomposition in a Static Reactions over SrO at the indicated temperatures. The Sample was preactivated at 1133 K. $P_{\text{N}_2\text{O}} = 2.5$ torr. Data taken by mass spectrometry.
(page 28)
- FIG. A-5a: Plot of Reciprocal Space Velocity (α contact time) vs. % Conversion at Reaction Temperature 740 K over SrO preheated to 1273 K for 6.0 hours in an Argon Flow. Data taken by Continuous-Flow, Gas Chromatographic Procedure.
(page 29)
- FIG. A-5b: Plot of LN Rate Vs. LN $P_{\text{N}_2\text{O}}$ Decomposition at 758 K over SrO Preactivated in an Argon Flow at 1273 K for 6 hours. Data obtained by continuous flow G.C. procedure.
(page 30)
- FIG. A-6a: Effect of Preactivation Temperature upon Kinetic Parameters for N_2O Decomposition at 758 K (Plot i, data points) and for Oxygen Isotope Exchange at 290 K over 50 mgm of SrO (Plot ii, data points). The Kinetic Parameter used as a measure of Catalytic Activity of the Preactivated Sample for Decomposition of $P_{\text{N}_2\text{O}} = 2.5$ Torr was the slope of plots similar to Fig. 4. For Oxygen Isotope Exchange the Kinetic Parameter utilised as a measure of Activity was $T_{\frac{1}{2}}$ for Isotopic Equilibration of an Initial Pressure of 0.1 Torr of ($^{16}\text{O}_2 + ^{18}\text{O}_2$) (cf. Fig. 8).
(page 31)
- FIG. A-6b: Effect of Preactivation Temperature (bottom axis) upon Steady State Activity of SrO for N_2O Decomposition at 758 K, as observed by Continuous-Flow G.C. Procedure with Input $P_{\text{N}_2\text{O}} = 380$ Torr.
(page 32)
- FIG. A-7: Profiles of the Initial Activity of SrO after Preactivation of three different Temperatures for the Conversion, $\text{N}_2\text{O} \rightarrow \text{N}_2 + \text{xO}_2$, at 758 K. Each Data Point represents % conversion to N_2 observed for individual pulse from the first pulse upward. Each pulse $\rightarrow \times 10^{-7}$ moles of N_2O and the bottom axis is the cumulative number of moles of N_2O introduced at $P_{\text{N}_2\text{O}} = 40$ Torr in the pulsed microcatalytic G.C. procedure. Plot (i), data points = activation at 993 K. Plot (ii), data points = activation at 1083 K; Plot (iii) data points = activation at 1273 K.
(page 35)

- FIG. A-8: Progress of the R_O -type Oxygen Isotope Exchange Process at 290 K over SrO Preactivated in Vacuo at 1223 K. Plots show the mole fraction of $^{16}O_2$ (^{32}X) and $^{18}O_2$ (^{34}X) decreasing with Time (Data Points ●) and the Mole Fraction of $^{16}O^{18}O$ (^{34}X) increasing (Data Points ■) with Contact Time in accordance with $^{16}O_2 + ^{18}O_2 \rightleftharpoons 2^{16}O^{18}O$.
(page 36)
- FIG. B-1: Results of computations showing the reconstruction ('rump1ing') of MgO surfaces having Ba^{2+} heavily segregated (to monolayer equivalent) to the surface. Numbers indicate (in lattice units) the outward displacement of two Ba^{2+} and two O^{2-} representing a unit cell of the reconstructed surface.
(page 58)
- FIG. B-2: Effect of Ba^{2+} surface dopant upon photoexcitation (Parts A and B) and luminescence emission spectra (Part C) relative to undoped MgO: 2A, Plot I, pure MgO, Plot II 3 m.e. Ba^{2+}/MgO ; 2B Dependence of excitation features at 340 nm upon following nominal loading of MgO surface by Ba^{2+} - 3.2 m.e. (A), 1.6 m.e. (B), 0.6 m.e. (C), 0.3 m.e. (D) and 0.06 m.e. (E); 2C Differences in spectral distribution of emission from pure MgO (plot I) and from 3 m.e. Ba^{2+}/MgO excited at 340 nm (plot II) or 280 nm (plot III).
(page 60)
- FIG. B-3: Excitation (Part A) and Emission (Part B) spectra at 293 K of unsupported BaO prepared from $BaCO_3$ and $Ba(NO_3)_2$; A(i) and (ii) respectively are excitation spectra of BaO prepared from $BaCO_3$ and $Ba(NO_3)_2$ monitored at emission wavelength = 460 nm; B(i) and (ii) are emission spectra of BaO, ex. $CaCO_3$ and $Ba(NO_3)_2$ respectively, excited at 335 nm.
(page 62)
- FIG. B-4: Effects of reducing gases (Part A) and oxidising gases (Part B) upon Ba^{2+} -related luminescence features of 3.2 m.e. Ba^{2+}/MgO : 4A photoexcitation spectra after: (I) enhanced outgassing; (II) contact with 10^{-2} torr H_2 ; (iv) upon evac. of H_2 ; (v) after 3h outgassing to 10^{-7} torr. 4B Extent of quenching of emission of 460 nm in the presence of indicated pressures of N_2O or O_2 at 300 K.
(page 65)

- FIG. B-5: Build-up of N_2 product from N_2O dissociation at 300 K over Ba^{2+}/MgO samples in static reactor:
(page 67)
- 5A: Relative rates of build-up over same 3.2 m.e. Ba^{2+}/MgO sample after preactivation at indicated temperatures.
- 5B: Relative Rates of Build-up over different samples having indicated nominal surface loadings of Ba^{2+} . All samples similarly preactivated at 1273 K.
- FIG. C-1: Auger spectra (a) nickel support after argon ion bombardment;
(page 73) (b) strontium deposited at $P = 2 \times 10^{-10} T$ ($\theta_{Sr} \approx 16.0$),
(c) oxidized at $P_{O_2} = 5 \times 10^{-7} T$ 300°C for 1.0 h, and outgassed for 0.3 h, at 300°C; (d) barium deposited on Ni/SrO ($\theta_{Ba} \approx 1.7$)
- FIG. C-2: Ratio of the intensity of the strontium auger peak to the nickel
(page 75) peak as a function of evaporation time.
- FIG. C-3: Work function change ($\Delta\phi$) as a function of barium coverage
(page 77) (θ_{Ba}) on strontium oxide.
- FIG. C-4: Auger spectra of (a) nickel support after argon ion bombardment;
(page 79) (b) barium deposited at $P = 6.0 \times 10^{-10}$ Torr ($\theta_{Ba} \approx 4.5$);
(c) barium oxidized at $P_{O_2} = 5 \times 10^{-7}$ Torr at 300°C for 1.0 hours and outgassed at 300°C for 0.3 hours and (d) barium deposited on Ni/BaO ($\theta_{Ba} \approx 7.0$).
- FIG. C-5: Intensity of the nickel auger peak as a function of barium
(page 80) evaporation time.
- FIG. C-6: Variation in work function (ϕ) as a function of barium coverage
(page 81) (θ_{Ba}) on barium oxide.

SECTION I

INTRODUCTION

This report describes and interprets results of new experimental studies made upon systems selected for their ability to model various important features of oxide cathodes and the mechanisms which enable them to function as efficient thermionic emitters at moderate temperatures.

Firstly, an account is given of experiments which aimed to simulate conditions upon the surfaces of polycrystalline samples of alkaline earth oxides (e.g. SrO and BaO/SrO or MgO and BaO/MgO) at various stages of their preparation in similar fashion to that used in the thermal activation of oxide cathodes. One novel feature of this group of experiments was the development of photoluminescence measurements in the wavelength region 270-500 nm as a surface-sensitive spectroscopic technique for probing changes in electronic energy levels of extrinsic surface states during thermal activation of mixed oxide systems. Recent computations on mixed-oxide systems such as BaO/MgO indicate a strong driving force for segregation of Ba^{2+} to the surface and for pronounced reconstruction (rumpling) of the surface monolayer - caused by the need to accommodate the large Ba^{2+} cations. A preliminary comparison is made between changes in electronic energy levels expected from such Ba^{2+} -related surface reconstruction and the changes in electronic energy levels inferred from photoluminescence measurements.

Secondly, accounts are given of experiments which examined the interaction between the gases O_2 , N_2O , H_2 or CH_4 and appropriately preactivated surfaces of pure and mixed alkaline earth oxide samples. Such experiments were of interest, not only in the context of improving

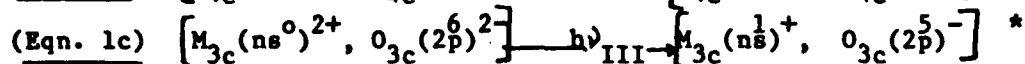
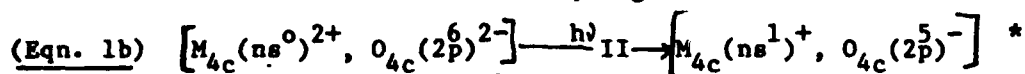
the understanding of how residual gases deactivate oxide-cathode surfaces, but also in assessing the value of the gases as 'molecular probes' possessing a capability for signalling the existence of particularly active surface sites at various stages in the activation/deactivation of alkaline earth oxide surfaces.

Thirdly, accounts are given of experiments involving the controlled deposition in UHV conditions of zero-valent Ba^0 ad-atoms - in amounts ranging from submonolayer to multilayer coverage - upon layers of SrO or BaO previously prepared in UHV conditions by evaporation of the corresponding metal and its subsequent oxidation. These experiments related particularly to the important role widely envisaged for a thin coating of Ba^0 species upon oxide cathode surfaces in minimising their work-function under steady-state operation. Measurements of work function changes with increasing coverage, θ_{Ba} , of the surface by Ba^0 thus represented an essential component of these studies and are reported for Ba^0 upon SrO and upon BaO layers.

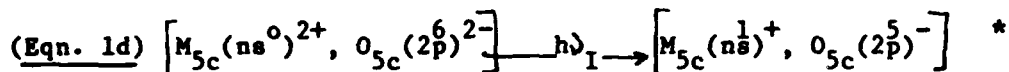
Finally, UPS spectra have been undertaken in order to examine surfaces of samples prepared by evaporation of barium metal or strontium metal and to study effects upon the UPS spectra by exposures to the gases N_2O , O_2 and CH_4 . The relevance of such reexamination of these systems by UPS stemmed from the following inferences drawn by earlier workers from their UPS studies of the oxidation of evaporated layers of barium or strontium: (i) diffusion of oxygen into the barium films with insignificant change (at the high energy end) in the UPS for very small O_2 (<13L) exposures

manner remains somewhat controversial, since the following difficulties/alternatives can be envisaged: (i) although large differences in Madelung potential have been advanced as an important contributory factor towards the 2-4eV red shifts of transitions ld, lc and lb relative to la, the adequacy of energy changes thereby attainable has been questioned on the basis that considerable relaxation/re-organisation would occur around extended topographical features such as steps. This would, relative to the unrelaxed cases, significantly diminish the differences in Madelung potential between relaxed location having degrees of co-ordinative unsaturation differing nominally by integers of point charge (12); (ii) proposals by Heinrich et al. on the basis of UPS evidence, that extrinsic surface states on surfaces of some single crystal oxides are attributable to cations left with diminished co-ordination through the creation of anion vacancies, i.e. at point defects rather than at extended topographical defects (13); (iii) demonstrations that large red-shifts, plus good correlation of transition energies with those of excitonic transitions, are not conclusive indicators of excitonic character. Indeed, for alkali halides, these features are exhibited to a marked degree by transitions involving the excitation of electrons trapped at point defects (14). Mindful of these differing possibilities, the method of presentation adopted throughout this series of papers will be, on the one hand to utilise as convenient working hypotheses existing models differentiating between surface-excitons on the basis of differing degrees of co-ordination at various (unspecified) surface locations, whilst on the other considering the extent to which other models, such as those involving point defects, and adsorbates, may likewise account for the observed results.

are at surface locations and do not enjoy full octahedral co-ordination (7,8). According to the interpretation espoused by Stone et al., features II and III in the reflectance spectra are to be associated with photo-generation of surface excitons involving ions having only four-fold or three-fold co-ordination, e.g.



Variation of these transition energies for the different alkaline-earth oxide in accordance with the Mollwo-Ivey relation for localised excitons lent support to the interpretation of features II and III in terms of localised surface excitons. However, the transition energies of feature I were observed to vary in similar fashion to freely diffusing excitons of the bulk and this has been assigned to photogeneration of surface excitons at surface locations involving ions having five-fold co-ordination, e.g.



Possibilities for migration of this type of surface exciton have been proposed (9) and will be examined experimentally in this sequence of studies by doping the surfaces of MgO, CaO and SrO with BaO. This latter should act as a trap for surface excitons of the host oxide, since BaO excitonic energy levels lie at lower energies than corresponding excitonic levels for the other oxides.

Interpretations favouring step-edges or corners as the surface topographical features mainly responsible for the existence of anions and/or cations with four-fold or three-fold co-ordination, have been strongly espoused not only by Stone and co-workers (see above) but also by Tench et al., (see below). Rigid interpretation in this

Introduction

Absorption features lying to the long wavelength side of their absorption edges, and attributable to the photogeneration of correlated electron-hole pairs within the lattice (i.e. 'bulk-excitons'), have been reported for single crystals of high-purity alkali halides (1,2) and for some alkaline earth oxides, (3,4). In terms of the tight binding approximation (generally considered applicable to these groups of highly ionic solids) such bulk-exciton transitions may be thought of as promoting an electron from an anion site enjoying full octahedral co-ordination onto similarly co-ordinated adjacent cation sites. Thus within the bulk of a perfect single crystal composed of M_{6c}^{2+} and O_{6c}^{2-} ions, the upward transition may be approximated by

(Eqn 1a) $[M_{6c}(ns^0)^{2+}, O_{6c}(2p)^{2-}] \xrightarrow{h\nu} [M_{6c}(ns)^1+, O_{6c}(2p)^{5-}]^*$

Emission of uv photons arising from the corresponding reverse transitions has been observed with many of these ionic solids (5,6).

Spectroscopic observations reported in the present series of papers for the isostructural alkaline earth oxides, MgO, CaO, SrO and BaO relate, however to other electronic transitions which are displaced to longer wavelength by 2-4eV relative to bulk-exciton transitions. These are most readily observable in samples of high surface area, such as powdered oxide samples prepared by thermal decomposition of the corresponding carbonates or hydroxides in vacuo at high temperatures. Careful reflectance measurements, mainly by Stone et al., have revealed three partially resolved absorption features, which they denote by I, II and III respectively and which they interpret in terms of 'surface excitons', i.e. transitions analogous to Eq. 1a, except that the anion and/or cation sites involved

Surface Reactivity and Spectroscopy Compared for Alkaline Earth Oxides:
Part I, Dependences upon Temperature of Preactivation for SrO

John Nunan, John A. Cronin and Joseph Cunningham,
(Chemistry Department, University College, Cork, Ireland).

ABSTRACT

High surface area samples of strontium oxide, prepared by thermal decomposition of high purity SrCO_3 in vacuo, have been examined for their reactivity/catalytic activity towards molecular gas probes and for luminescence spectra. Temperature profiles are reported, as a function of prior outgassing temperature, for the development of room-temperature excitation and emission spectra. These are compared with temperature profiles for the development of room-temperature catalytic activity for R_O -type oxygen isotope exchange, $^{16}\text{O}_2 + ^{18}\text{O}_2 \rightleftharpoons 2^{16}\text{O}^{18}\text{O}$, and for development of activity for nitrous oxide decomposition, at various temperatures. Consideration is given to interpretations of the results in terms of ions at co-ordinatively unsaturated surface locations, to the extent to which these are exposed after thermal activation at various temperatures, and to the involvement of point defects in the surface locations responsible for the various surface processes.

APPENDIX A

TITLE: *Spectroscopic and Kinetic Studies of Surface Processes on
Alkaline Earth Oxides
Part I: Strontium Oxide Preactivated at various Temperatures*

NAMES: John Cronin, John Nunan & J. Cunningham

A Paper based on these results has been submitted to J.Chem.Soc.(London),
Faraday Transactions, for publication.

oxidized layer to ca. 500°C in UHV restored intensity into the -1.5 V feature relative to that at -3 V, in a manner consistent with restoration of a surface composition having regions of metallic barium plus dispersed/isolated O^{2-} species. Such indirect support for the existence of regions of barium metal was all that could be arrived at in this UPS since since direct observation of metallic-like photoemission at E_F of barium metal was not accessible due to lack of provision for applying electrical bias to the sample and to presumably very low work function of barium metal regions of the surface.

For reasons just given, direct observation of the metallic-like emission from Sr^0 was not accessible. Photoemission features of bulk SrO or of chemisorbed oxygen were expected to be accessible in UPS of Sr^0 / SrO prepared by evaporations from a commercial strontium evaporator onto a tantalum source. Our experiments showed only the growth of a rather broad (width at half height .3V) UPS feature peaking at ca. -3.5 V relative to the E_F position initially measured for tantalum and indicating some SrO formation. Additional broadenings of this band upon exposures to N_2O (50 L) or O_2 (50-100 L) at room temperature were consistent with further oxidation towards stoichiometric SrO . Subsequent heating of the oxidised layers up to 600°C in vacuo caused this latter broad band to be replaced by a narrow UPS feature peaking at ca. -2.5 V relative to the position measured for E_F of tantalum. This sharp UPS feature was reminiscent of a strongly favoured photoemission identified in the literature with O^{2-} species dispersed in a surface layer of Sr^0 . This feature at -2.5 V w.r.t. E_F tantalum was not removed by exposure to gaseous CH_4 (3000 L) at 600°C.

coverage from "break-point" plots upon the AES features of Ba^0 (cf. fig. C-2) Results of these procedures for the $\text{Ni}/\text{SrO}/\text{Ba}^0$ system (cf. figure C-3 of Appendix C) demonstrate clearly an initial sharp drop in work function as θ_{BaO} increased to ca. 0.2 monolayer equivalents, followed by a flat plateau wherein no further reduction of ϕ with θ_{Ba} occurred while the latter increased to ca. 0.7 m.e., at which coverage the work function rose towards the value characteristic of metallic barium. The results confirm experimentally the important role of submonolayer coverages by Ba^0 in bringing about and maintaining a sizeable reduction of work function of the SrO surface - such as has been widely proposed to be essential for stable, long-term operation of oxide cathodes. Qualitatively dissimilar effects were observed with the $\text{Ni}^0/\text{BaO}/\text{Ba}^0$ model systems prepared and examined in similar manner. The probable origins of this anomaly are being considered in view of observed effects of visible light and of subsequent measurements made on this system by the group of T.W. Haas at WPAFB.

4. TYPE IV Studies (relating to UPS measurements upon surfaces of evaporated barium or strontium layers and changes caused therein by exposures to N_2O , O_2 and CH_4).

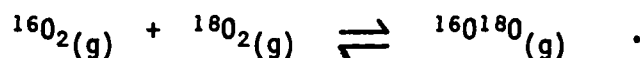
Evaporation of barium onto a 'clean' tantalum foil substrate, which initially allowed the observation of photoemission from d-band states of E_F of tantalum, resulted in its replacement by a double humped photoemission band, the two components of which peaked at -1.5 and -3V relative to that measured previously for E_F of tantalum and were attributable to a partially oxidised barium layer. (Partial oxidation resulted from insufficiently good vacuum during the evaporation process). Exposure of this partially oxidised Ba/BaO layer to 10^{-5} torr O_2 at room temperature strongly enhanced the feature at -3V relative to that at -1.5 V, in a manner consistent with transformation of the surface regions more completely towards bulk BaO and away from an initial surface composition including region of metallic barium, into (or onto) which some O^{2-} was dispersed. Subsequent heating of the

flow mode after large exposures to N_2O were not sensitive to, nor suitable for, detecting effects of surface defects - witness the fact that the ratio of N_2 to O_2 product took values of 2.0 ± 0.1 in such experiments.

3. TYPE III Studies (*relating to changes induced by zero-valent Ba^0 ad-atoms at submonolayer to multilayer coverage in the Work Function and ESCA of UHV-prepared substrates including SrO and BaO . See Appendix C for full details of these experiments*).

Clean, chemically well-defined systems, designed to study surface and interfacial properties of '*Nickel Substrate/Alkaline Earth Oxide/ Ba^0 monolayer*', arrangements which are of likely importance in the operation of oxide cathodes, were prepared as follows in an UHV system equipped for XAES: (i) thermal outgassing and argon ion bombardment of a nominally pure nickel foil, until XAES of the foil yielded the AES spectrum appropriate to a 'clean' nickel metal surface, i.e. freed from all but minor residual traces of carbon and sulphur (*cf. figure C-1*); (ii) Evaporation of multilayer amounts of Sr^0 (or Ba^0), characterized by the AES appropriate to Sr metal, onto the clean nickel substrate followed by oxidation in high purity oxygen to yield an oxidized layer with AES appropriate to SrO (or BaO); (iii) periodic, carefully-controlled evaporation of Ba^0 atoms onto the oxide layer, interspersed by XAES measurements in UHV which allowed semi-quantitative evaluation of θ_{Ba} , the surface coverage by Ba^0 and of accompanying changes in the work function of the oxide surface; (iv) Parallel control evaporations (in identical geometric configuration and with equal voltage supplied to the Barium metal evaporator) so as to allow identification of monolayer

Another gas-phase conversion which proved to be valuable as a 'molecular probe' for active surface sites 'frozen-in" upon alkaline earth oxide surfaces following preactivation at high temperatures was the oxygen isotope equilibration process.



Following preactivation in vacuo at sufficiently high temperature > 1023 K, strontium oxide, SrO (ex SrCO_3) surfaces exhibited varying degrees of activity for this process when an equimolar mixture of $^{16}\text{O}_2$ and $^{18}\text{O}_2$ was introduced at room temperature. An approximately linear dependence of the extent of room temperature activity upon temperatures of preactivation above 1023 K (*cf. plot ii of figure A-6a*) measured for SrO surfaces shows important differences from temperature profiles for development of photoluminescence features. The differences could be consistent either, with less crucial importance of degree of coordination of ions at the surface for reactions of molecular probes thereon than for photoluminescence from the same surface, or alternatively with insensitivity of the rate determining step for surface reaction towards the degree of coordination of surface oxide ions.

Evidence for an important role of surface defects in the conversions of molecular-probe molecules upon the surfaces came from studies of the dissociation of N_2O over SrO (ex SrCO_3) surfaces at 758 K. Using both continuous-flow and pulsed-reactant techniques involving gas chromatography with thermal conductivity detection, clear evidence for defect-aided incorporation of oxygen fragments (from $\text{N}_2\text{O} \rightarrow \text{N}_2 + \text{O}$) into the oxide lattice emerged from strong upward deviation in the ratio of N_2 to O_2 product, but only in the pulsed reactant mode (*cf. figure A-7*).

Steady state rates of decomposition observed in the continuous-

2. Type II Studies (relating to interactions of 'probe' gas molecules, - including O_2 , N_2O , CH_4 and H_2 - with thermally preactivated surfaces of polycrystalline alkaline-earth oxides. Appendices A and B should be consulted for full details of these experiments).

Reference has already been made (cf. fig.B-4b) to the strong quenching effect which low pressures of O_2 and N_2O exerted upon photoluminescence at room temperature from surface regions of Ba^{2+}/MgO samples which had previously been thermally activated in vacuo at 1273 K.

Quenching by O_2 was fully reversible and disappeared when the O_2 was evacuated at 300 K, whereas only ~70% of the quenching effect of N_2O was removed by such evacuation. Decomposition of N_2O to give N_2 (but no O_2) product in the gas phase was shown by mass spectrometry to occur at preactivated $Ba^{2+}/MgO - N_2O$ interfaces in the same condition which gave irreversible quenching of photoluminescence (cf. fig. B-5 of Appendix B). It was concluded that quenching involved the destruction of luminescence centres by reaction at 300 K with the oxygen fragment from N_2O decomposition. Conversely, the totally reversible nature of the quenching by molecular oxygen pointed to only non-dissociative interaction of O_2 at 300 K with the luminescence centres upon preactivated Ba^{2+}/MgO surfaces.

Reversible effects upon photoluminescence at room temperature from preactivated Ba^{2+}/MgO were also observed with H_2 and CH_4 , but these hydrogen-containing reducing gases caused some enhancement of luminescence and so contrasted strongly with the quenching effects noted above for the oxidising gases O_2 and N_2O at 300 K.

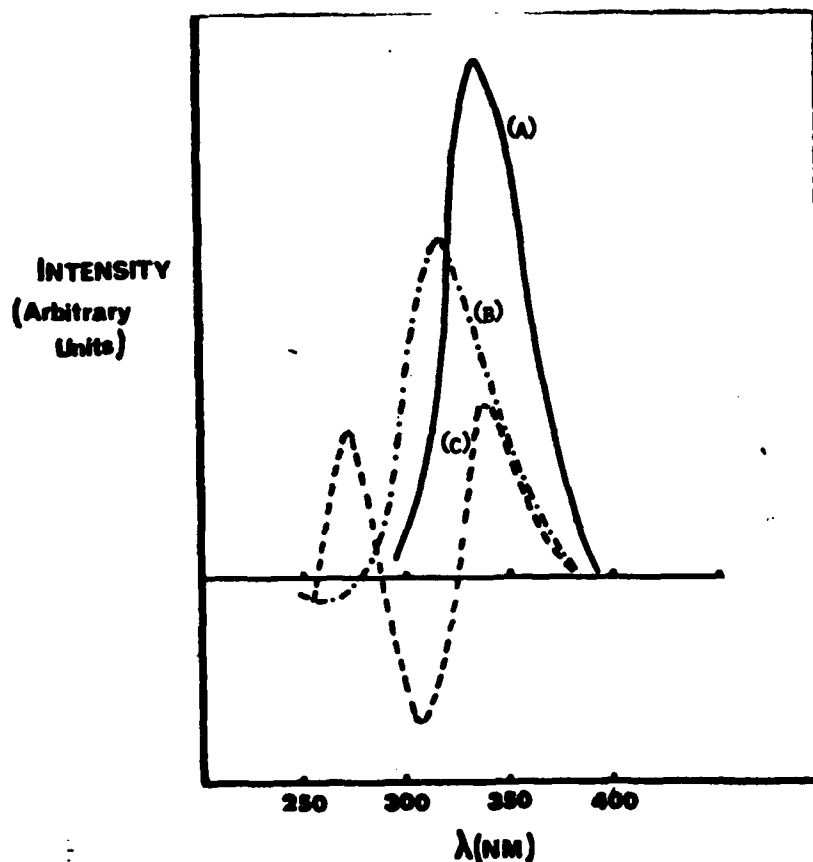


FIGURE 1 : Difference Excitation Spectra for BaO/MgO, Plot (A), BaO/CaO, Plot (B) and BaO/SrO, Plot (C). All samples at loading >3 m.e.

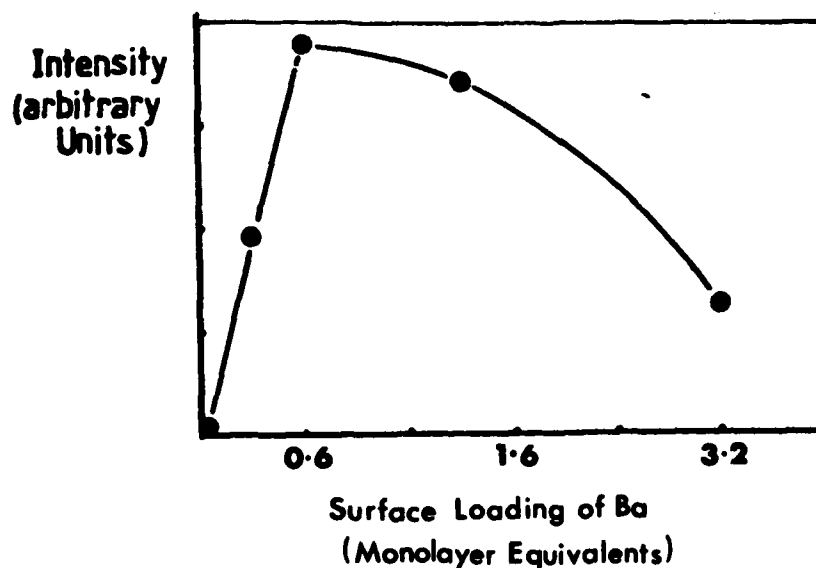


FIGURE 2 : Variation of Relative Intensities of Ba^{2+} -related Emission with $\lambda_{(\text{max})} = 460$ nm from $\text{Ba}^{2+}/\text{MgO}$ samples having the Indicated Nominal Surface Loadings (monolayer equivalents) of Ba^{2+} ($\lambda_{\text{ex}} = 335$ nm).

sensitivity of these Ba^{2+} -related luminescence features to quenching by small pressures of O_2 or N_2O (cf. figure A-4) that the sites from which this luminescence originated were predominantly located at the surfaces of these $\text{Ba}^{2+}/\text{MgO}$, $\text{Ba}^{2+}/\text{CaO}$ and $\text{Ba}^{2+}/\text{SrO}$ samples.

The differential photoexcitation spectra shown in figure 1 illustrate the extent to which the Ba^{2+} -related surface luminescence from these materials could be separated (on the basis of differing λ_{max} and/or differing spectral distribution) from luminescence of the corresponding undoped oxide. Excellent separability is clearly achieved for $\text{Ba}^{2+}/\text{MgO}$. That for $\text{Ba}^{2+}/\text{CaO}$ might also form the basis of a spectroscopic method for evaluating the *surface* concentration of Ba^{2+} . However, the $\text{Ba}^{2+}/\text{SrO}$ system, which approaches most closely to the likely situation at the surface of oxide cathodes (particularly when non-operational after long periods of prior use), clearly would pose much greater problems for reliable assessment of surface Ba^{2+} concentration, $[\text{Ba}^{2+}]_s$, on the basis of differential photoexcitation spectroscopy (d.px.s.) based only upon differences in spectral distribution. Data in Fig. 2 show that at large differences in luminescence *intensity* between pure and Ba^{2+} -doped MgO surfaces could represent another basis for determining $[\text{Ba}^{2+}]_s$ on $\text{Ba}^{2+}/\text{MgO}$ by d.px.s., at least up to ca. 0.6 monolayer equivalents of Ba^{2+} . The ending in 1983 of our access to the luminescence spectrometer prevented investigation of the applicability of intensity-based d.px.s. to determination of $[\text{Ba}^{2+}]_s$ on $\text{Ba}^{2+}/\text{SrO}$ materials, or actual oxide-cathode layers.

SECTION II

SUMMARY - RESULTS AND CONCLUSIONS

1. TYPE I Studies *(relating to thermal activation of pure and mixed alkaline earth oxide powders and photoluminescence measurements thereon. Appendix A should be consulted for full details of these experiments).*

Completion of the conversion $\text{SrCO}_3 \rightarrow \text{SrO}$, with elimination of the last traces of the aragonite structure of the carbonate (monitored by IR of the solid), and virtual disappearance of CO_2 from the off-gases (monitored by mass spectrometry) was demonstrated to require temperatures in excess of 1073 and approaching 1173 K.
(cf. figures A-1 and 2).

A strong correlation existed between the temperature dependences evident in figs. A-1 and A-2.

The latter were attributable to increasing availability of coordinatively unsaturated $\text{Sr}_{\text{cus}}^{2+}$ and $\text{O}_{\text{cus}}^{2-}$ ions at the surface as residual CO_3^{2-} and CO_2 were progressively removed. In the photoexcitation spectrum the new feature corresponded to a band with λ_{max} at 315 nm, whilst in photoemission λ_{max} was at 450 nm, *(cf. figure A-2a, A-2b).*
of these features was achieved after outgassing of the SrO powder at temperatures 1173-1273 K.

Although powdered BaO prepared from BaCO_3 yielded extremely weak photoluminescence, the impregnation of soluble barium salts onto the surfaces of SrCO_3 , CaCO_3 or Mg(OH)_2 , followed by their activation in vacuo at 1273 K, yielded intense new photoluminescence features whose intensities varied in proportion to the level of doping of the surfaces by Ba^{2+} .
(cf. figure B-1 of Appendix B). It could be concluded, on the basis of strong

and work function changes less than 0.1 eV; (ii) development at O_2 exposures $13 \rightarrow 200$ L of atom-like O^{2-} isolated species upon Ba, such O^{2-} being characterized by an unusually narrow UPS feature ca. 5 V below E_F and by the fact that it did not attenuate a small metallic-like component in the UPS; (iii) transition at higher O_2 exposures to a thick-oxide BaO layer, characterized by a UPS feature of half width ca. 2.75 eV, still centered around 5 V below E_F ; (iv) existence of a large number of crevices in the BaO thick-oxide layer, as inferred from persistence of the metallic-like (alkaline earth d-state) emission up to rather large O_2 exposures and from an accompanying increase in reactivity (sticking coefficient) for O_2 . This latter observation led to a suggestion that exposure of fresh Ba^0 surface accompanied the growth of BaO oxide up to a cut-off thickness because of stress at the BaO/Ba interface due to structural mismatch (the Ba is bcc while the oxide is fcc and moreover the barium-barium distance is shorter in BaO). Inferences similar to (i) \rightarrow (iii) above have been drawn in the literature from UPS studies of the oxidation of evaporated Sr layers but with the following differences in emphasis; (v) retention of a metallic layer at the surface of the oxidised layer at exposures up to 160 L was more explicitly demonstrated on the basis of only minor changes in work function; and (vi) changes in activity (towards O_2 during initial oxide growth) were smaller and occurred over a much smaller range of oxygen uptake than for Ba/BaO.

Much of the published studies of surface processes upon high surface area samples of alkaline-earth oxides prepared by decomposition of the corresponding oxyanion salts has demonstrated rather strong dependences of luminescence (9) and of surface reactivity (15) or catalytic properties (16,17) upon the temperature and duration of sample outgassing. Thus maximum activity for the isomerization of 1-butene to cis- and trans- 2-butene was reported for MgO samples pretreated at 873 - 973K (16a) whereas the maximum activity for the hydrogenation of olefines was reported following evacuation at 1373K (16b). It has further been found, in comparison of the abilities of oxygen, hydrogen, ammonia or n-buthylamine to act as poisons, that different selectivities emerged for poisoning various types of reaction over the same oxide catalyst. Thus over BaO, oxygen poisoned more selectively the exchange reaction of butene with deuterium than the isomerization reaction (17a). In the case of 1-butene isomerization over SrO (17b) n-butylamine and ammonia poisoned preferentially the formation of trans-2-butene. At higher outgassing temperatures hydrogen treatment resulted in the retardation of the formation of cis-2-butene while trans-2-butene was retarded by oxygen treatment. Such observations strongly suggested: the existence of a variety of active sites upon alkaline earth metal oxides; that some of these sites were only fully developed following high temperature pretreatments, such as would remove the final traces of CO₂ and H₂O from the surface (18); and that only a fraction of the surface was active for the observed catalysis. The active sites have been variously attributed (19) to Lewis acid-base sites involving, respectively, cations and oxygen ions with various degrees of co-ordinative unsat-

uration, (M_{cus}^{2+}) and (O_{cus}^{2-}). Strong similarities may be noted between these attributions and those in the working hypotheses of Stone and Tench outlined above in connection with luminescence. This first paper in our series explores the degree of correlation between temperature dependences of surface reactivity and surface luminescence for Strontium oxide. Subsequent papers will examine the influence of BaO as a surface dopant upon the luminescence and the surface reactivity of SrO and CaO.

Experimental

Vacuum Procedures: Both the thermal decomposition of strontium carbonate to SrO and its subsequent activity for N_2O decomposition and O_2^{16}/O_2^{18} exchange were studied in a static quartz reactor using conventional vacuum procedures with mass spectrometric analysis. In order to follow the progress of the thermal decomposition of high purity $SrCO_3$ ('Spex' spectroscopically pure grade) in the quartz reactor, powdered sample was slowly heated to 1273K over a period of ten hours, during which the total pressure was monitored and the gas composition of gaseous decomposition products determined by leaking samples to a VG Micro Mass 6 mass spectrometer via a leak valve. Nitrous oxide was supplied by B.D.H. Chemicals and had a purity of greater than 99%. Before contacting $P_{N_2O} \sim 3.5$ torr with the catalyst, the gas was further purified by a series of freeze-pump-thaw cycles, after which purity was further checked by leaking the gas into the Micro Mass 6 through a by-pass valve. With the SrO catalyst at temperatures in the range 673 - 873K, reaction was initiated by admitting purified N_2O and periodically obtaining the mass spectrum of gas samples leaked into the Micro Mass 6. Reaction temperature and

catalyst mass were chosen such that the reaction time for 50% conversion was greater than ten minutes. Under these conditions the reaction rate was found not to be limited by diffusional effects.

For oxygen isotopic exchange studies, an isotopically non-equilibrated mixture consisting of 50% O_2^{16} + 50% O_2^{18} was employed (Norsk Hydro). This gas was contacted with the catalyst at room temperature. The mass spectrometric procedure was the same as for N_2O decomposition, but oxygen pressures in the range 0.1 to 0.01 torr were used. In general SrO was activated prior to reaction by heating under vacuum to the required activation temperature and maintaining this temperature for one hour before cooling to room temperature in vacuo. Base pressure in the vacuum system employed was 5×10^{-6} torr.

Gas Chromatographic Procedures: Nitrous oxide decomposition was also studied using g.l.c. and microcatalytic flow reactor system operating at atmospheric pressure. A feature of these studies was the use of both the continuous-flow and pulsed-reactant procedures and full details have elsewhere been given illustrating its use in both modes (20). Strontium carbonate samples (200 mg) were decomposed in situ in the quartz microcatalytic reactor by heating at different temperatures up to a maximum of 1273K for 1.0 hours in a flow of dry helium at a flow rate of 40 mls. per minute. Prior to the admission of nitrous oxide as pulses, or as a continuous flow, the catalyst temperature was lowered to the reaction temperature. The reactor was then isolated while N_2O/He mixtures were prepared such that the pressure of N_2O took values in the range 50 to 250 torr. The total flow rate was then restored to 40 mls. per minute.

Luminescence Procedures: Instrumentation used in obtaining the excitation/emission spectra has previously been described in detail (9). Excitation was provided by a 250 W Xenon lamp from which appropriate wavelengths were sequentially selected using two coupled Spex f4 monochromators whilst taking excitation spectra. A single Spex monochromator placed between sample and detector was held at a fixed wavelength and augmented by appropriate cut-off filters in taking excitation spectra. Spectra were automatically corrected for variations in excitation intensity with time or changing wavelength via instrumental comparisons (with an Ortec photon-counting system) of the pulse rates from two monochromators: one monitoring luminescence intensity and the other the intensity of the source at the same wavelength. Excitation spectra at acceptable signal/noise ratio were only obtained upward from 230 nm, due to low source intensity at shorter wavelengths. Sharp cut-off filters (Corning 3-74 and 0-52) were placed between the sample and the emission monochromator to minimise scattered wavelengths from the Xenon source reaching the photomultiplier. A band-pass of 5 nm was used for both the excitation and emission results.

RESULTS

Decomposition profiles of SrCO_3 as a function of the outgassing temperature are summarised in Figure 1. Using total pressure of gaseous products as the monitor shows that the carbonate started to decompose at -873K, reached a maximum at 1023K and was almost complete at 1073K. Mass spectrometric analysis shows that the major decomposition products were CO_2 and CO, as shown in Figure 1(b), but that some water vapour was also present. The ratio of CO/CO_2 changed markedly

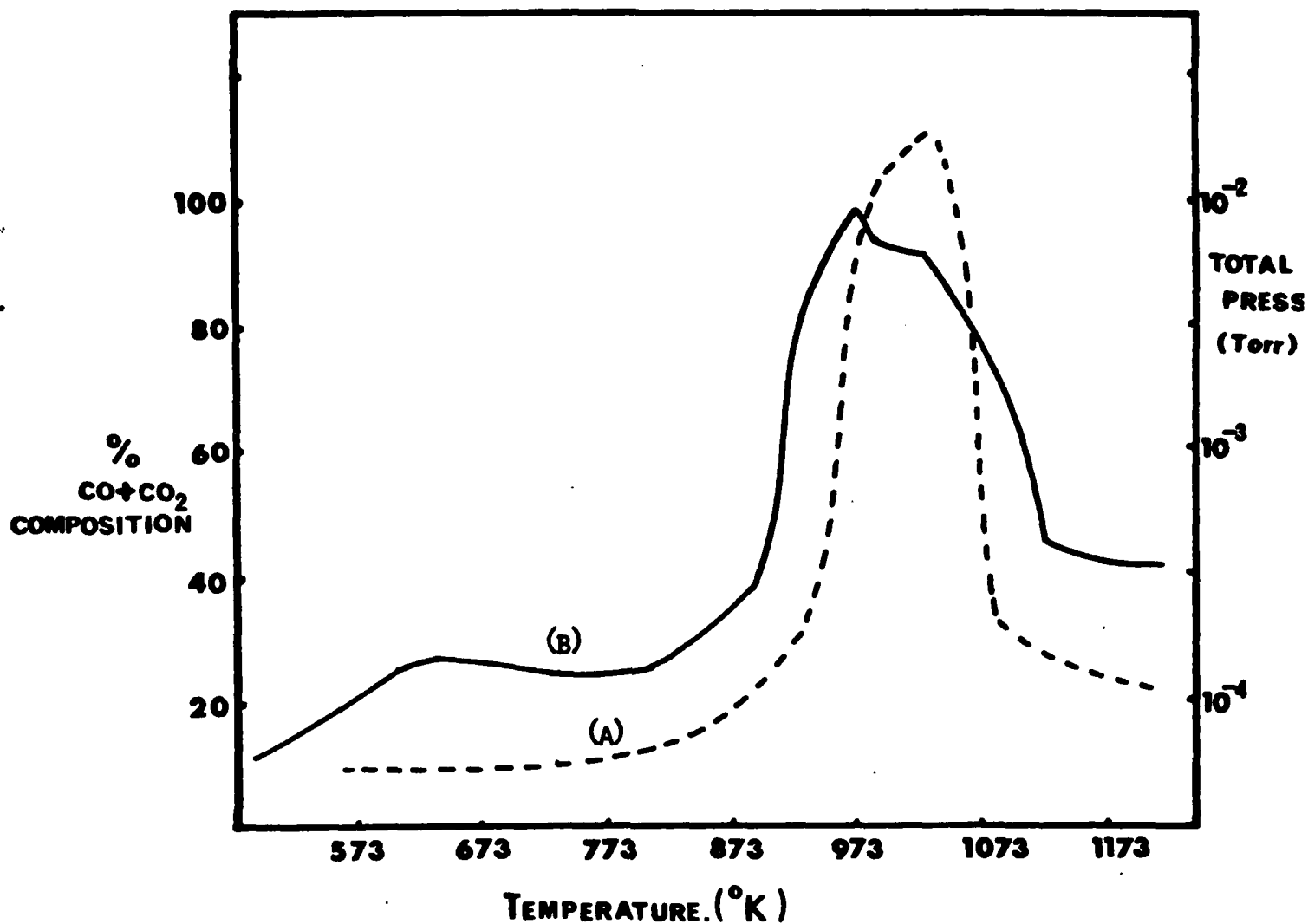


FIGURE A-1 a & b

STUDY OF SrCO_3 DECOMPOSITION AS A FUNCTION OF OUTGASSING TEMPERATURE

A = CO + CO₂ COMPOSITION IN GAS PHASE ABOVE THE SAMPLE

B = TOTAL PRESSURE OF DECOMPOSITION PRODUCTS OVER THE SAMPLE

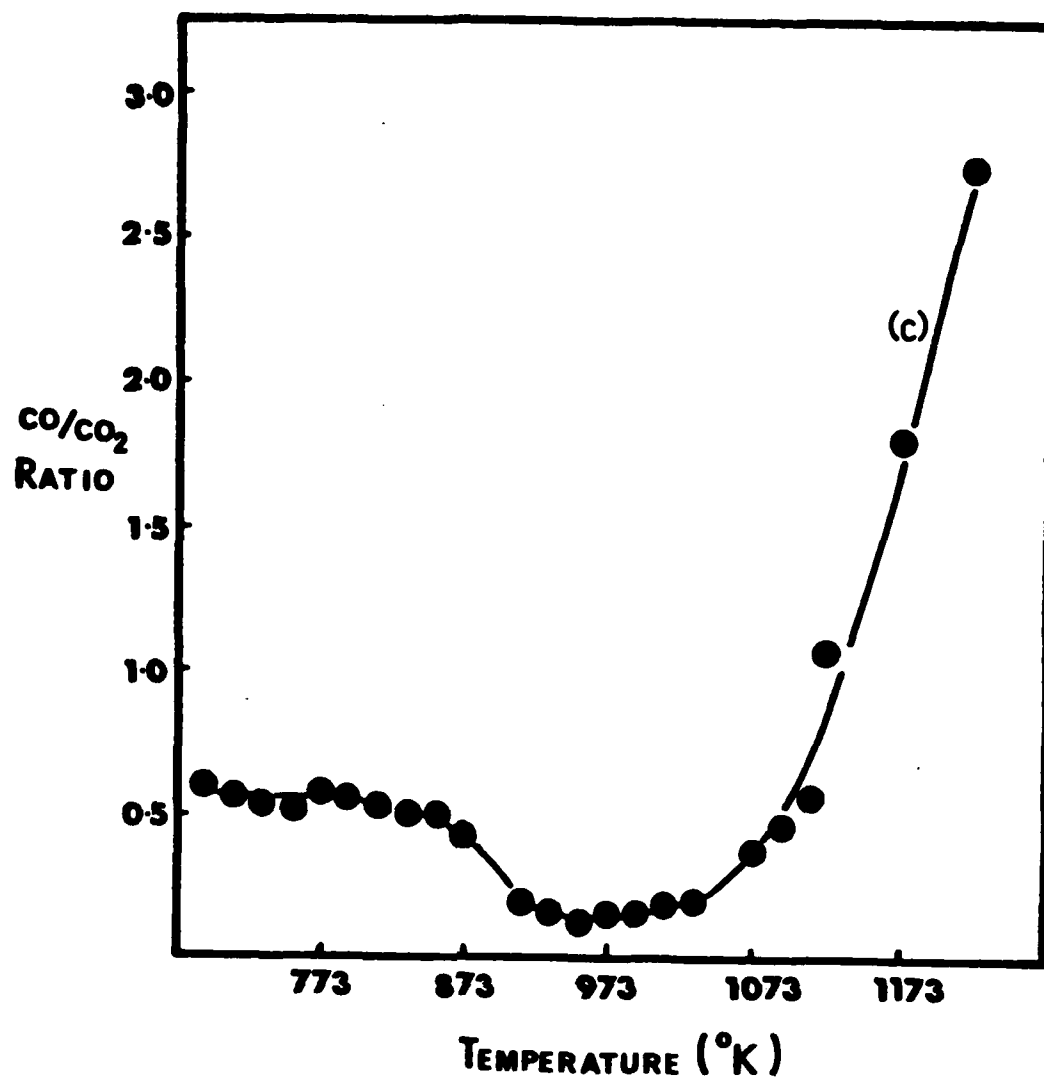


FIGURE A-1 c

PLOT OF CO/CO₂ RATIO IN THE DECOMPOSITION PRODUCT AS
A FUNCTION OF OUTGASSING TEMPERATURE FOR SrCO₃.

as the activation temperature was increased above 1073K, with CO becoming the dominant decomposition product at the high temperatures (cf. Fig. 1c).

Effects of prior outgassing at different temperatures on the emission/excitation spectra of SrO at room temperature are shown in Figure 2. The excitation/emission spectra appeared only upon outgassing above 1073K. Further increases in outgassing temperature brought about a progressive increase in the emission peak intensity and an accompanying increase in excitation peak intensity. Increasing the outgassing temperature also brought about significant changes in the peak shape and position. Thus in the excitation spectra, both a peak at 280 nm and an accompanying shoulder at 315 nm were observed to grow and experience changes in relative intensity in going from 1023 to 1273K (cf. Figure 2A, plots (i), (ii), (iii) and (iv)). Upon outgassing for 4.0 hours at 1293K the relative intensity in the latter shoulder was observed to decrease again (cf. Fig. 2A(v)). Parallel observations upon the emission of the same sample showed that outgassing at 1023K led to two broad peaks centered at 400 and 455 nm (cf. Figure 2B(i)). Outgassing at the higher temperature of 1223 and 1273K resulted in a single peak at 465 nm, as shown in Figure 2B, plots (iii) and (iv). However, extensive outgassing at 1293K for 4.0 hours led to a shift in the emission maximum back to 450 nm and a reduction in its intensity of ca 40% (plot (v) Fig. 2B).

Figure 3 illustrates the effects of exciting the emission at different excitation wavelengths for a SrO sample first outgassed at 1023 and then at 1293K. It is clear that for the sample pre-treated in different fashions the emission peak shape and position remained

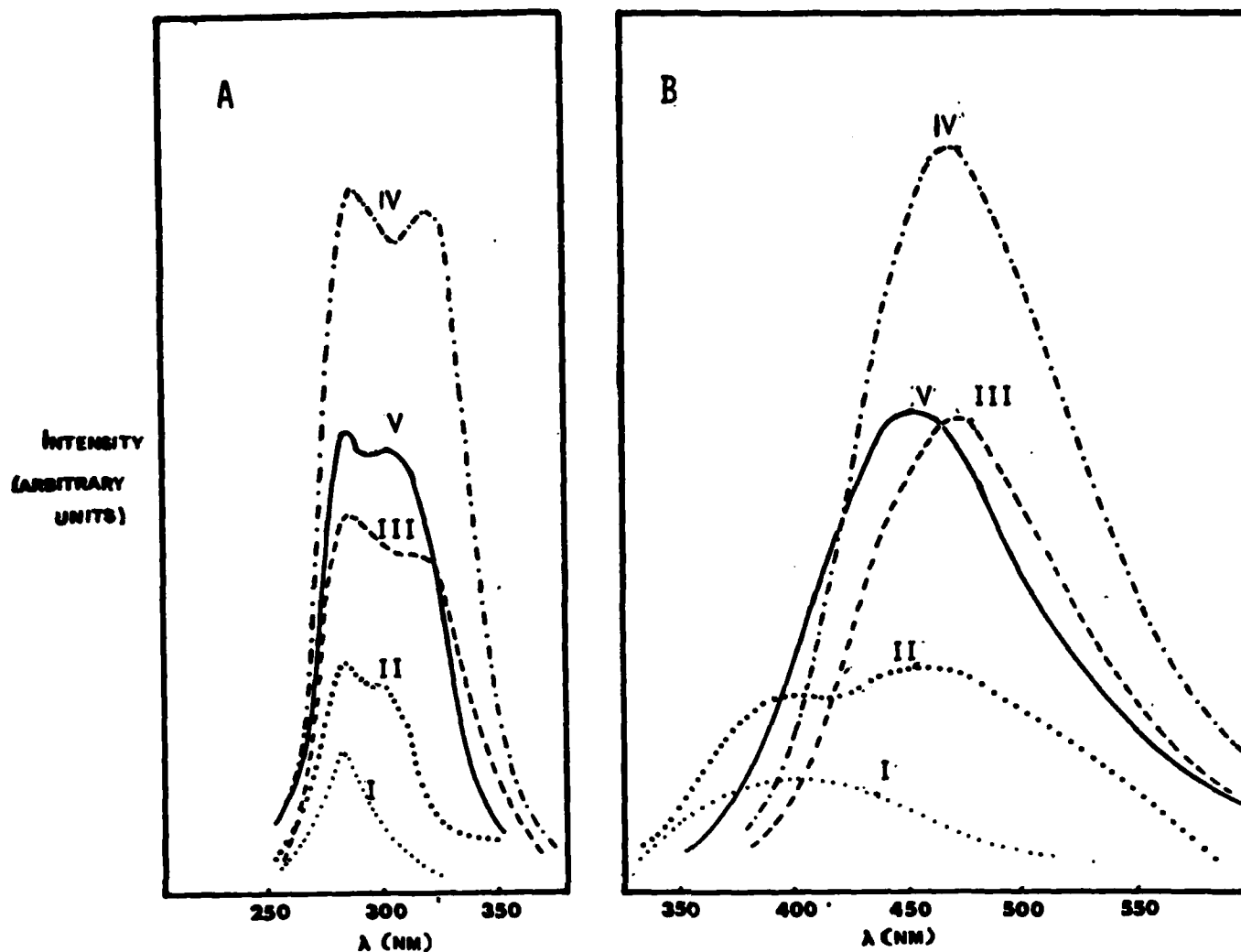
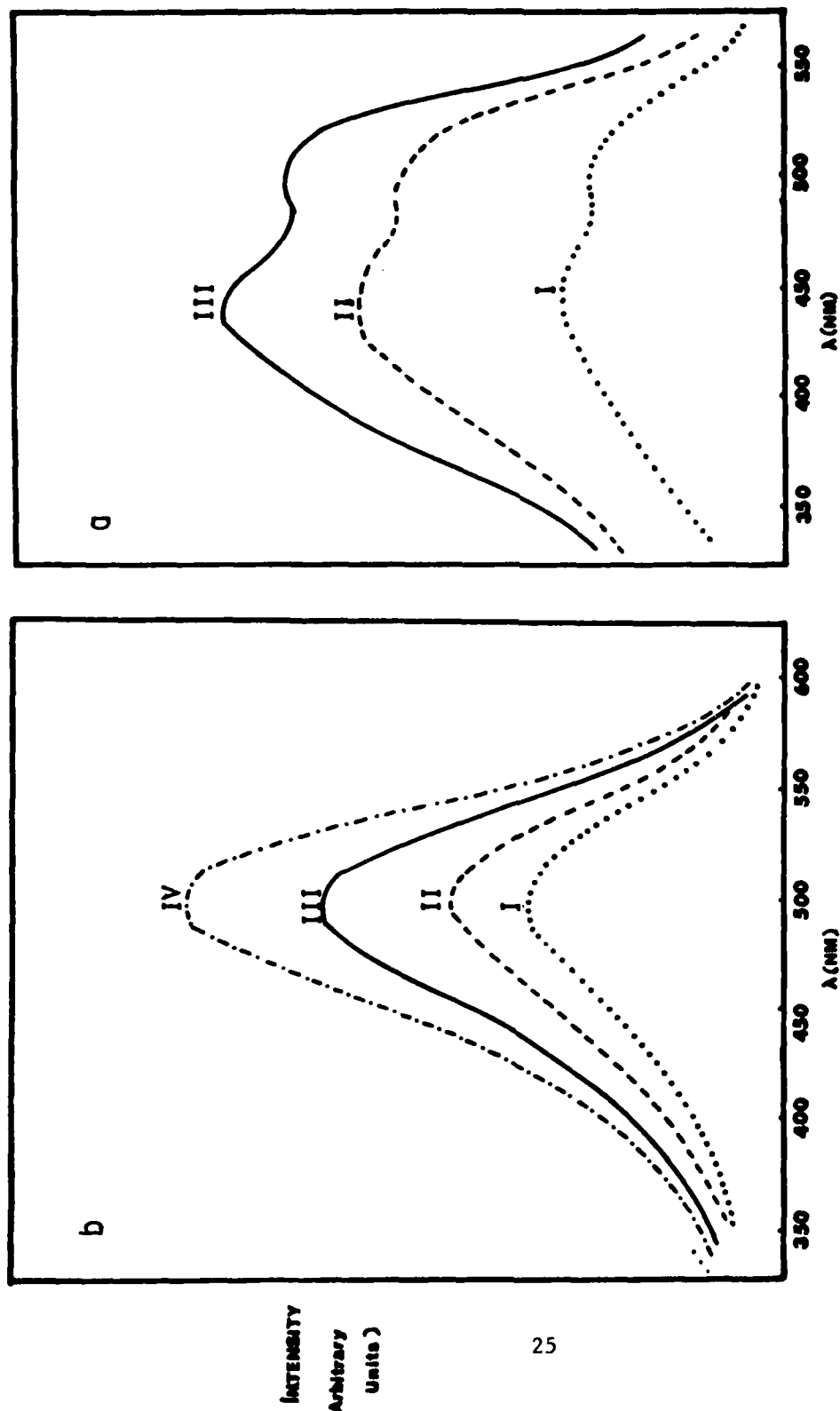


FIGURE A-2

EXCITATION SPECTRA (FIG. A-2a) and Emission Spectra (FIG. A-2b) of SrO (ex SrCO_3) OUTGASSED AT VARIOUS TEMPERATURES BETWEEN 1073 K AND 1293 K: A(i) AND B(i) EXCITATION AND EMISSION SPECTRA RESPECTIVELY FROM SrO OUTGASSING FOR ONE HOUR AT 1073 K; A(ii) AND B(ii) SPECTRA AFTER OUTGASSING FOR ONE HOUR AT 1123 K; A(iii) AND B(iii) SPECTRA AFTER OUTGASSING AT 1123 K FOR ONE HOUR; A(iv) AND B(iv) SPECTRA AFTER OUTGASSING AT 1173/1273 K FOR ONE HOUR; A(v) AND B(v) SPECTRA AFTER OUTGASSING AT 1293 K FOR FOUR HOURS.

A-3
FIGURE 3



EMISSION SPECTRA OF SrCO_3 EXCITED BY DIFFERENT WAVELENGTHS OF EXCITING LIGHT AFTER OUTGASSING AT 1073 (FIG. 3A) AND 1293 K (FIG. 3B); PLOTS A(I) AND B(I) ARE EMISSION SPECTRA OBSERVED UNDER EXCITATION AT $\lambda = 280$ NM FROM SrO OUTGASSED AT 1073 AND 1273 K RESPECTIVELY; A(II) AND B(II) EMISSION SPECTRA EXCITED AT $\lambda = 299$ NM FROM SrO OUTGASSED AT 1073 AND 1273 K RESPECTIVELY; A(III) AND B(III) EMISSION SPECTRA EXCITED AT $\lambda = 315$ NM FROM SrO OUTGASSED AT 1073 AND 1293 K RESPECTIVELY; B(IV) EMISSION SPECTRA EXCITED AT $\lambda = 325$ NM FROM SrO OUTGASSED FOR ONE HOUR AT 1173/1293 K.

independent of the exciting wavelength. This was also found to be the case for samples outgassed at 1223 and 1273K.

These excitation and emission results agree well with those obtained by Coluccia et al. (9). In excitation the band having max at 280 nm, similar to that previously attributed by Coluccia to five-coordinate surface positions, appeared first. The other weaker band with max at 315 nm, similar to that attributed by Coluccia to four-coordinate surface locations, only developed as outgassing temperature increased towards 1273K. In emission, the bands shown in Fig. 2B as the first to develop in our spectra with max at 400 and 450 nm, are very similar to those assigned by Coluccia to emission from surface locations involving five-fold and four-fold co-ordination respectively. The development of emission with max at 465 nm only after outgassing at the higher temperatures, as illustrated by Fig. 2B iii, had previously been interpreted in terms of the involvement of surface ions with three-fold co-ordination. Furthermore, our observation that, regardless of whether excitation of SrO outgassed at the higher temperatures was made at 280 or 315 nm, emission was dominated by the band at 450 nm reproduces observations made earlier by Coluccia et al. and attributed by them to energy transfer from sites of five-fold co-ordination (excited by photons having 280 nm and emitting at 400 nm) to sites of four-fold co-ordination (excited by photons having 315 nm and emitting at 450 nm).

Catalytic Results

Nitrous oxide decomposition at temperatures 673 - 873K over SrO samples pretreated in the ways indicated was found to follow first-

order kinetics, whether studied by the mass spectrometry procedure or the gas chromatographic procedure. In Figure 4 are shown the first-order plots of N_2O decomposition at 677, 656 and 683K obtained using mass spectrometry. Linear regression analysis gave correlation coefficients ranging from 0.992 - 0.997 for the three plots. For the gas chromatographic continuous-flow studies kinetic data were obtained under conditions where the reactor was operating in the differential mode. This was achieved by selecting the reaction temperature catalyst mass and flow conditions such that the conversions were less than 4%. Plots of the reciprocal space velocity versus conversion within this range were found to be linear, as shown in Figure 5A. Consequently the percentage conversion gives a direct measure of the rate of reaction. Applying the method of plotting of $\ln \text{Rate}$ vs. $\log P_{N_2O}$, the reaction could be shown to be first order with respect to N_2O pressure in the pressure range 50 to 250 torr, as illustrated in Figure 5B. In this manner first order kinetics in N_2O decomposition were shown to be obeyed over SrO ($exSrCO_3$) preactivated at various temperatures in the temperatures range 773 to 1273 K, independent of whether the reaction was studied using Mass Spectroscopy or g.l.c.

The effect of outgassing temperature on the reaction rate is summarized in Figures 6A and 6B where the first-order rate constants obtained using m.s. and g.c. are respectively plotted versus outgassing temperature. It is evident from Fig. 6B that, while some steady-state activity for N_2O decomposition became apparent after outgassing at 800 K, the rate only began to increase rapidly after outgassing at temperatures >1073 .

The use of the gas chromatographic procedure in its pulsed-reactant mode allowed investigation to be made of any progressive changes brought about in sample activity by contacting a preactivated

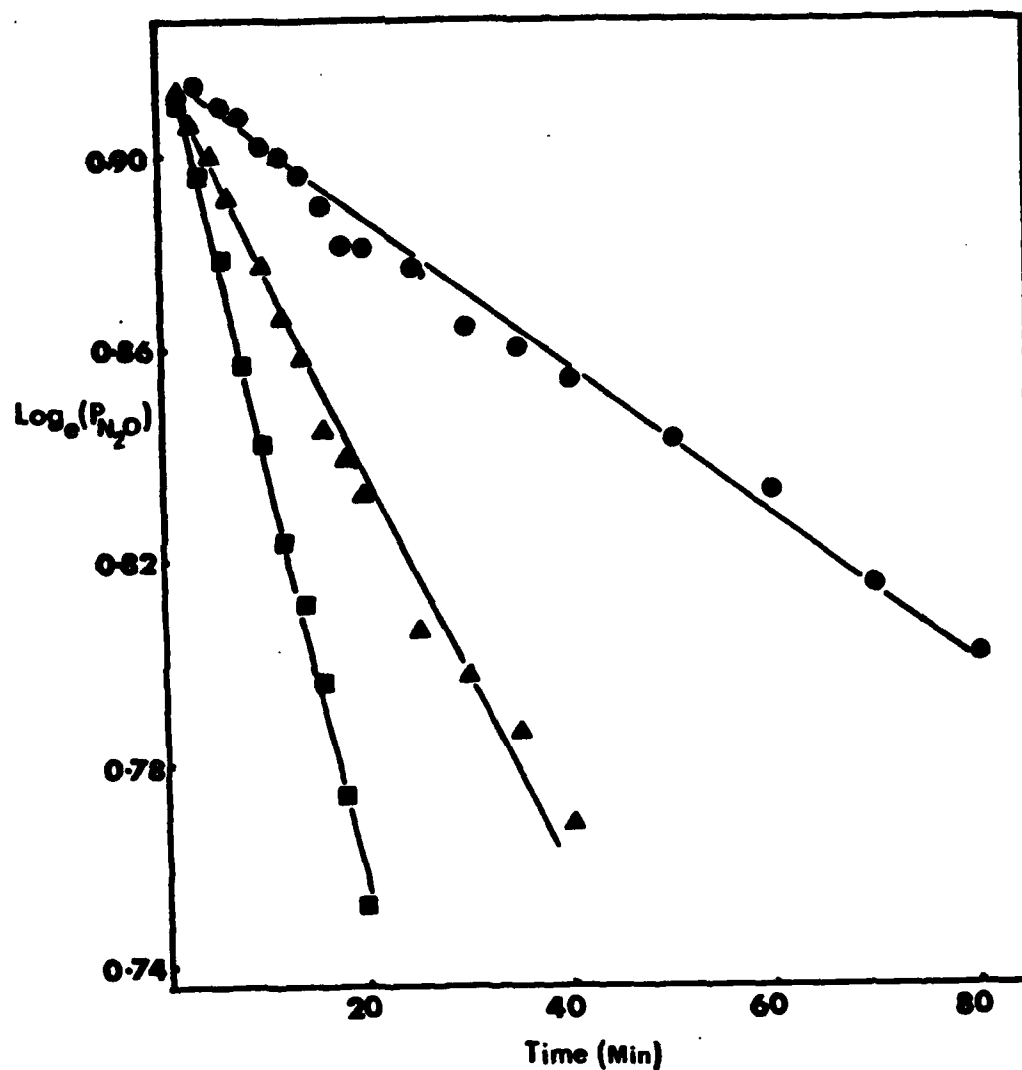


FIGURE A-4

FIRST ORDER PLOTS FOR N_2O DECOMPOSITION IN A STATIC REACTOR
OVER SrO AT THE INDICATED TEMPERATURES. THE SAMPLE WAS PRE-
ACTIVATED AT 1133 K. $P_{N_2O} = 2.5$ TORR.
DATA TAKEN BY MASS SPECTROMETRY.

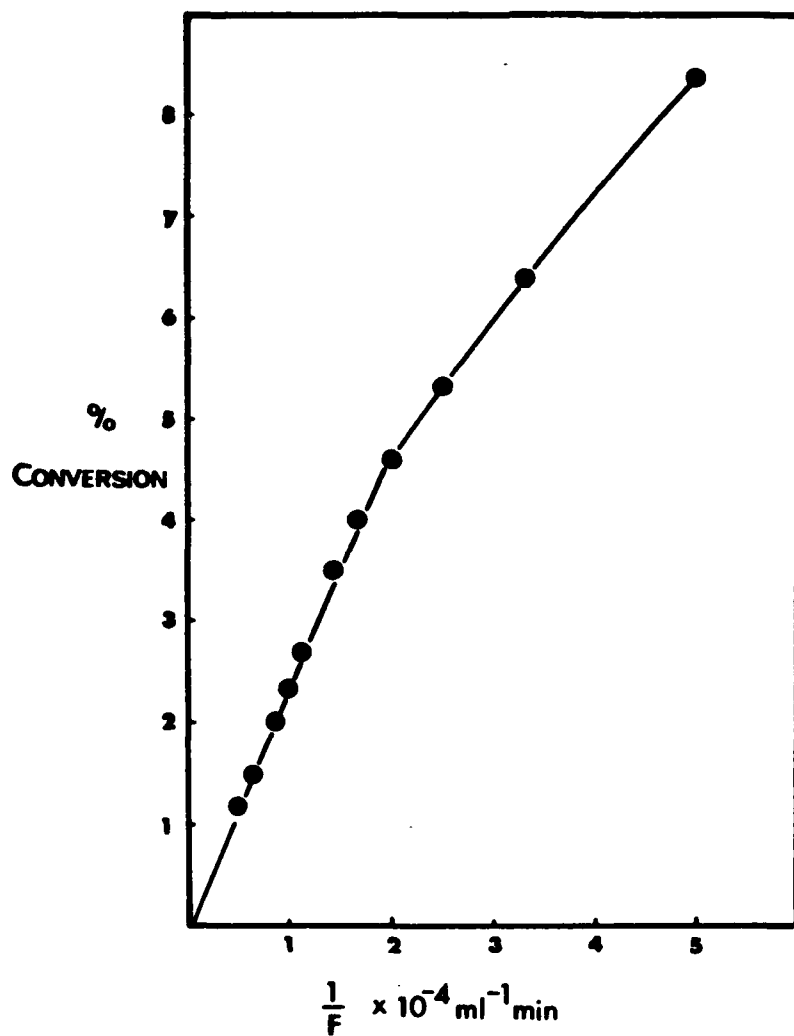


FIGURE A-5

PLOT OF RECIPROCAL SPACE VELOCITY (\propto CONTACT TIME) VS.
 % CONVERSION AT REACTION TEMPERATURE 740 K OVER SrO
 PREHEATED TO 1273 K FOR 6.0 HOURS IN AN ARGON FLOW.
 DATA TAKEN BY CONTINUOUS-FLOW GAS CHROMATOGRAPHIC
 PROCEDURE.

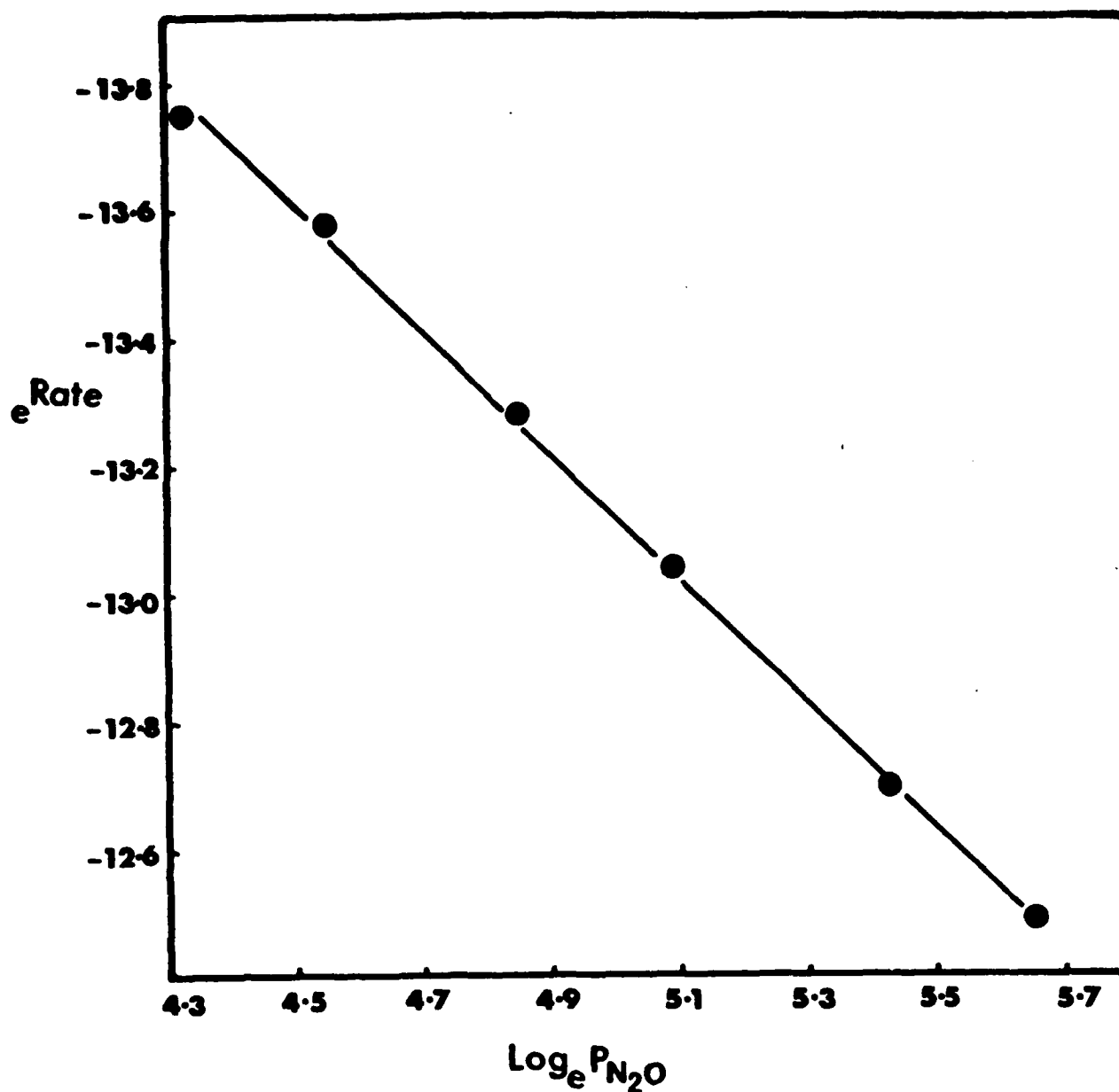
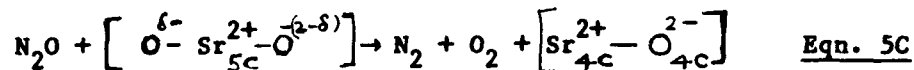


FIGURE A-5b

PLOT OF \ln RATE VS. $\ln P_{N_2O}$ DECOMPOSITION AT 758 K OVER SrO
PREACTIVATED IN AN ARGON FLOW AT 1273 K FOR 6 HOURS,
DATA OBTAINED BY CONTINUOUS FLOW G.C. PROCEDURE.

oxygen product generated in the pulsed procedure; and (ii) the possibility for regeneration throughout the interval between pulses.

Neither of the advantages just enumerated for the pulsed procedure apply with comparable force to results obtained for N_2O decomposition over SrO by the continuous flow g.c. procedure (cf. Figs. 5B and 6B). Nevertheless good mass balance with N_2/O_2 ratio = 2, together with stable steady-state conversions, were observed ⁱⁿ continuous-flow condition up to cumulative oxygen yields several orders of magnitude greater than in the pulsed procedure. These observations require some alternative to limited oxygen anion migration into the bulk as the process for regenerating Sr_{cus}^{2+} from sites blocked by oxygen product. In view of the large dynamic pressure of nitrous oxide ($P_{N_2O} = 380$ torr) to which the surface was continuously exposed, and in line with suggestions in the literature (26, 28), a likely alternative regenerative process is reaction of blocked sites with nitrous oxide as follows:

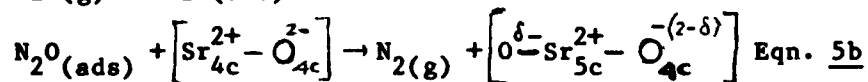


When taken in conjunction with eqn. 5b as a necessary preceding step, this regeneration process can account for the observed N_2/O_2 ratio of 2.0 and for the continuation of steady-state catalysed dissociation up to high turnover. Within this context, the strong dependence of steady-state activity upon the temperature of preactivation (cf. Fig. 6B) may be understood in terms of the necessity for preactivation at $T > 1000$ K for development and/or unblocking of the Sr_{4c}^{2+} sites necessary to initiate this two-step dissociation process. However, the contrast between expected levelling off in process 5b at relatively low N_2O

dissociation decaying rapidly to zero within the first 10 pulses of reactant, also implies an irreversible nature of step 5b and the non-operation, on surfaces preactivated at 1083 K, of secondary processes capable of regenerating active Sr_{4c}^{2+} locations through removal of oxygen fragments from process 5b.

The initial activity profile illustrated by the top plot of Fig. 7 for a sample preactivated at 1293 K demonstrates, not only the higher initial activity maximum expected on the basis that more Sr_{4c}^{2+} and some Sr_{3c}^{2+} sites would be exposed by this more rigorous preactivation, but also the retention of high activity up to high pulse numbers. This latter implies that preactivation at 1293 K had opened up pathways to surface processes via which the blocking effect otherwise resulting from process 5b was reversed. Our observation that the N_2/O_2 ratio rose to 3.8 over the sample preactivated at 1293 K effectively rules out removal of all of the oxygen product fragments of eqn. 5b to the gas phase as O_2 . However, the literature provides support for the likelihood of diffusion of a significant fraction of these fragments into the interior of the SrO crystallites. This recent calculation by Jacobs and Vempate (24) indicate a relatively low activation energy of 0.59 eV for anion interstitial migration in SrO. Earlier thermopower observations upon extrinsic diffusion in O_2/SrO systems were consistent with migration of anion interstitials or of cation vacancies (25) but the much higher value, 1.98 eV, recently calculated for the latter (24) would favour the anion interstitial interpretation. Operational features of the pulsed experiments which also appear particularly compatible with operation of oxygen ion migration as the mechanism for regeneration of $\text{Sr}_{\text{cus}}^{2+}$ were: (1) the small amount of

mode (Fig. 6B), or in the static reactor by mass spectrometry (Fig. 6A). In the g.c. pulsed mode, the first pulses N_2O encounter a surface bearing coverage, $\theta_{CO_3^{2-}}$ determined by the prior outgassing temperature. According to earlier arguments, pretreatment at 993 K, as per the bottom plot of Fig. 7, would leave some 5-co-ordinate sites still occupied by CO_3^{2-} as well as all of the 4 and 3-co-ordinate sites. The very low activity then observed, plus its rapid decline to zero after only a few pulses (Fig. 7), appears fully consistent with representation of the $SrO(993\text{ K})$ surface as remaining largely blocked by the adsorbed CO_3^{2-} . Treatment at 1083 K could be expected to desorb CO_3^{2-} not only from most 5-co-ordinate but also from some 4-co-ordinate sites (cf. eqn. 3), thus leaving them available for interaction with N_2O . Significantly the relevant initial activity profile (middle plot in Fig. 7) does then show a much larger maximum, as would be consistent with an important role of 4-co-ordinate sites in N_2O dissociation via equations 5a and 5b.



Since much of the driving force for abstraction of the oxygen from N_2O in 5b would originate from the degree of coordinative unsaturation of Sr_{4c}^{2+} , and since it has been proposed above that this can be partially satisfied by residual chemisorbed carbonate, the possibility cannot be excluded that proximate pairs of coordinatively unsaturated cations (e.g. $Sr_{4c}^{2+} - Sr_c^{2+}$ exposed across a step or dislocation at the SrO surface) may be required for 5b, rather than an isolated

$\left[Sr_{4c}^{2+} - O_{4c}^{2-} \right]$ location. The middle plot of Fig. 7, showing activity for N_2O

the basis of a static Madelung potential which ignored relaxation (8). However, to be effective in this respect, and so to help resolve the difficulty presently encountered in attempts to rationalise transition energies in terms of surface excitons, it would be necessary that coordination of carbonate onto M_{cus}^{2+} can diminish the drive towards relaxation whilst not significantly reducing the effective charge on adjacent anions. The extent to which these requirements may be met by various adsorbate configurations is the subject of ongoing calculations in these laboratories. Another feature of the luminescence results, which can well be accounted for in terms of the surface exciton model with some stabilization of M_{cus}^{2+} and O_{cus}^{3-} by chemisorbed carbonate, is the eventual erosion at 1293 K of the 465 nm emission band attributed to surface excitons involving ions nominally of three-fold coordination. Within the context of our hypothesis, the cations of such sites would in fact carry stabilizing carbonate-type adsorbate at least up to 1200 K and eqn. 1C should be modified accordingly. Further heating of the samples to sufficiently high temperature to drive off carbonate residue could then be expected to allow relaxation at sites thereby denuded. The observed erosion of the emission at 465 nm after long outgassing at 1300 K (cf. Fig. 2Bv) and the shift of the emission maximum back towards higher energy corresponds qualitatively to what might be expected from such relaxation.

Related interpretations can be developed for the observed dependences of N_2O dissociation upon the temperatures of preactivation in the range 900 - 1300⁰K (cf. Figs. 6A and 6B). It will be important to distinguish adequately between the likely surface condition whilst taking results in the g.c. pulsed mode (Fig. 7), the continuous flow

view, important implications for the degree of relaxation which may occur as surface defects develop during thermal preactivation of the powdered samples. Thus a residue of carbonate or other $(\text{CO}_3)^{2-}$ type adsorbate upon $\text{Sr}_{\text{cus}}^{2+}$ may serve to "pin" pairs or larger groupings of proximate $\text{Sr}_{\text{cus}}^{2+}$ and so inhibit them (23) from undergoing relaxation of the types predicted for 'clean' defect surfaces in theoretical calculations (22). Arguments will be developed below to the effect that preservation of $\text{Sr}_{\text{cus}}^{2+}$ at approximately their unrelaxed positions as a consequence of such pinning may materially assist in explaining present results and in diminishing difficulties which otherwise arise. It is important to preface these arguments by two general points: firstly, the validity of acknowledging the existence of adsorbates on these high surface area samples during their development by thermal pretreatments at base pressures $\geq 10^{-6}$ torr and secondly that, although present arguments can conveniently be developed in terms of carbonate-type adsorbate, pinning of coordinatively unsaturated surface cations through interaction with other surface adsorbates or impurity species may likewise be important.

In respect of luminescence results, possibilities for reconciling observed transition energies with various theoretical considerations arise from our hypothesis that residual carbonate-type adsorbate can stabilize surface cations in approximately their unrelaxed configurations. This may help remove the apparent anomaly between, on the one hand, theoretical calculations which predict extensive relaxation for coordinatively unsaturated locations on 'clean' surfaces (22), and on the other, the semi-quantitative agreement between observed and calculated energies for surface excitons achieved by Stone et al. on

Fig.2

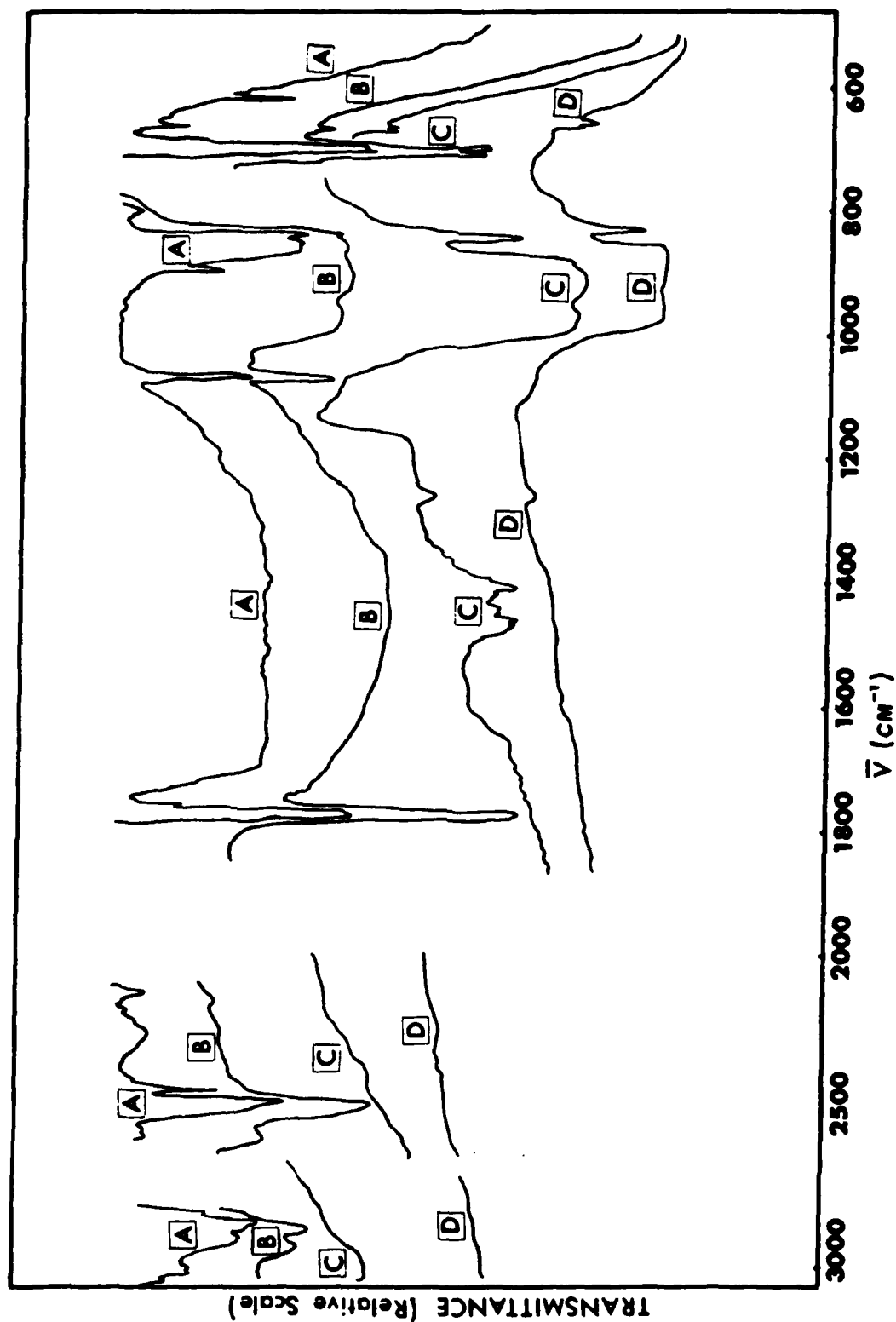
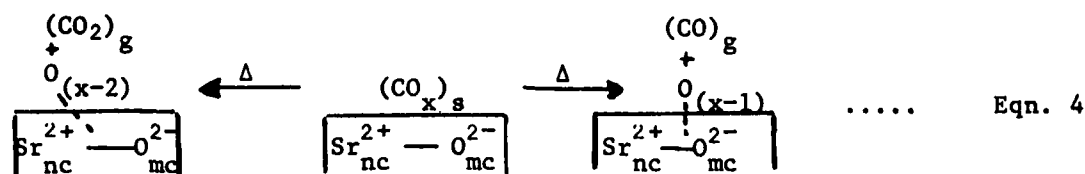


FIG. A-9: IR (at 293 K) of $\text{SrCO}_3 \rightarrow \text{SrO}$ conversion after 1 h vacuum outgassing at : (A), 293 K; (B), 973 K; (C), 1073 K; and (D), 1173 K.

outgassed at varying temperatures in a vacuum cell permitting in situ spectra (cf. fig 19). These showed the disappearance of detectable (bulk) carbonate IR absorption at ca. 1023K(20). The contrast between copious release at $T < 1073$ and the much smaller evolution of CO_2 persisting across the temperature range 1073 to 1273 K, may most readily be understood in terms of the onset across that temperature range of the more difficult release of $(\text{CO}_x)_s$ from surface sites of four or three-fold co-ordination. It has been argued elsewhere that such sites will be of much smaller abundance than five co-ordinate sites (9). It should also be recalled here that Fig. 1B demonstrated across the same temperature range a sharp increase in the CO/CO_2 ratio in the evolved gases. This suggests that, in parallel with desorption, an additional tendency existed for the more highly co-ordinatively unsaturated surface locations to break up $(\text{CO}_x)_s$ species (ions) in the following general way :



This particular schematic representation was selected for convenience in making clear how such transformation would account for our observations of an admixture of CO and CO_2 in the gas phase. However, it also serves to illustrate the surface configurations needed to accommodate possibilities that residual carbonate, or other $(\text{CO}_x)_s$ species, may : (i) exist bridged across a few co-ordinatively unsaturated surface cations and, (ii) give rise directly to carbon monoxide i.e. without the need for the appearance of completely unblocked $\text{Sr}^{2+}_{(n+1)\text{cus}}$ in significant numbers during the thermal preactivation of the sample. These latter possibilities carry, in our

ation has, where applicable, already been noted in the results section. Questions of particular relevance in this discussion are: firstly, whether remaining aspects of the results may likewise be understood within some elaboration of these existing hypotheses; and secondly, whether and to what extent the foregoing results might be understood in the context of alternative hypotheses on the nature of active surface.

Implicit within the existing hypotheses is the idea that the strength of bonding of adsorbates, such as CO_2 , N_2O or O_2 , would be lowest upon locations involving $\text{Sr}_{5\text{c}}^{2+}$ and/or $\text{O}_{5\text{c}}^{2-}$, intermediate upon those involving 4-co-ordinate surface ions and highest upon those involving 3-co-ordinate surface. Within this context it would be reasonable to consider that surface carbon-oxygen compounds, $(\text{CO}_x)_s$, which represent the precursors of the CO_2 and CO eventually released to the gas phase, can likewise exist at various surface locations which feature lattice cations and/or anions having varying degrees of coordination. The stronger bonding of $(\text{CO}_x)_c$ expected for 3-coordinate surface

sites, would favour retention of $(\text{CO}_x)_s$ to highest temperature on those sites, and to intermediate temperatures upon 4-co-ordinate surface sites. More facile release of $(\text{CO}_x)_s$ would be expected from 5-co-ordinate surface sites, which indeed seem likely to be involved in the normal, final step for release to the gas phase of CO_2 produced during thermal decomposition of SrCO_3 to SrO . Evidence for the partial completion of this relatively facile process at 1073K in the present study comes not only from the rapid drop in P_{CO_2} detected mass spectrometrically at that temperature (cf. Fig. 1), but also by a series of transmission IR spectra taken on a self-supporting disc prepared from SrCO_3 and

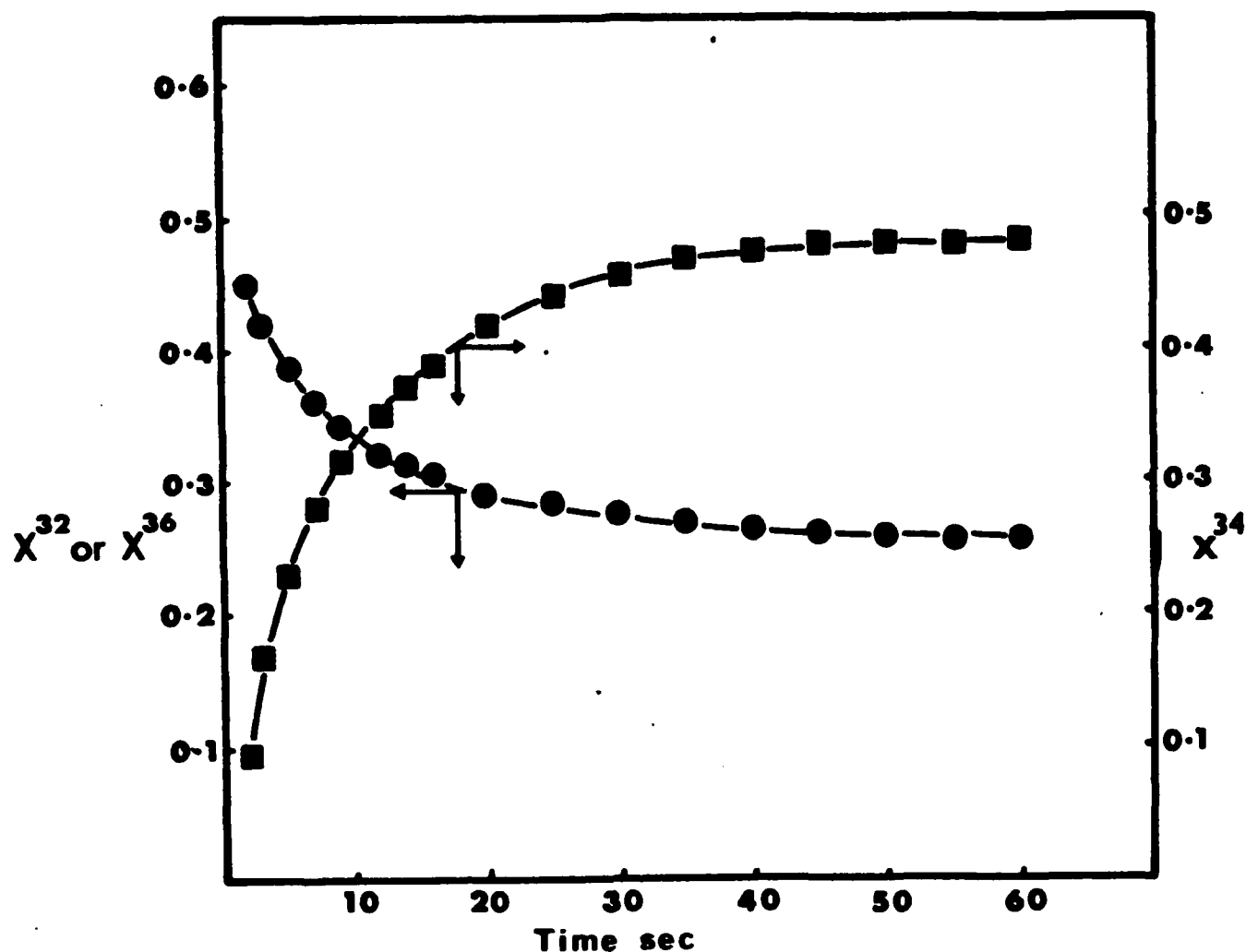


FIGURE A-8

PROGRESS OF THE R_0 -TYPE OXYGEN ISOTOPE EXCHANGE PROCESS AT 290 K OVER SrO PREACTIVATED IN VACUO AT 1223 K. PLOTS SHOW THE MOLE FRACTION OF $^{16}\text{O}_2$ (X^{32}) AND $^{18}\text{O}_2$ (X^{34}) DECREASING WITH TIME (DATA POINT \bullet) AND THE MOLE FRACTION OF $^{16}\text{O}^{18}\text{O}$ (X^{34}) INCREASING (DATA POINT \blacksquare) WITH CONTACT TIME IN ACCORDANCE WITH $^{16}\text{O}_2 + ^{18}\text{O}_2 \rightleftharpoons 2^{16}\text{O}^{18}\text{O}$.

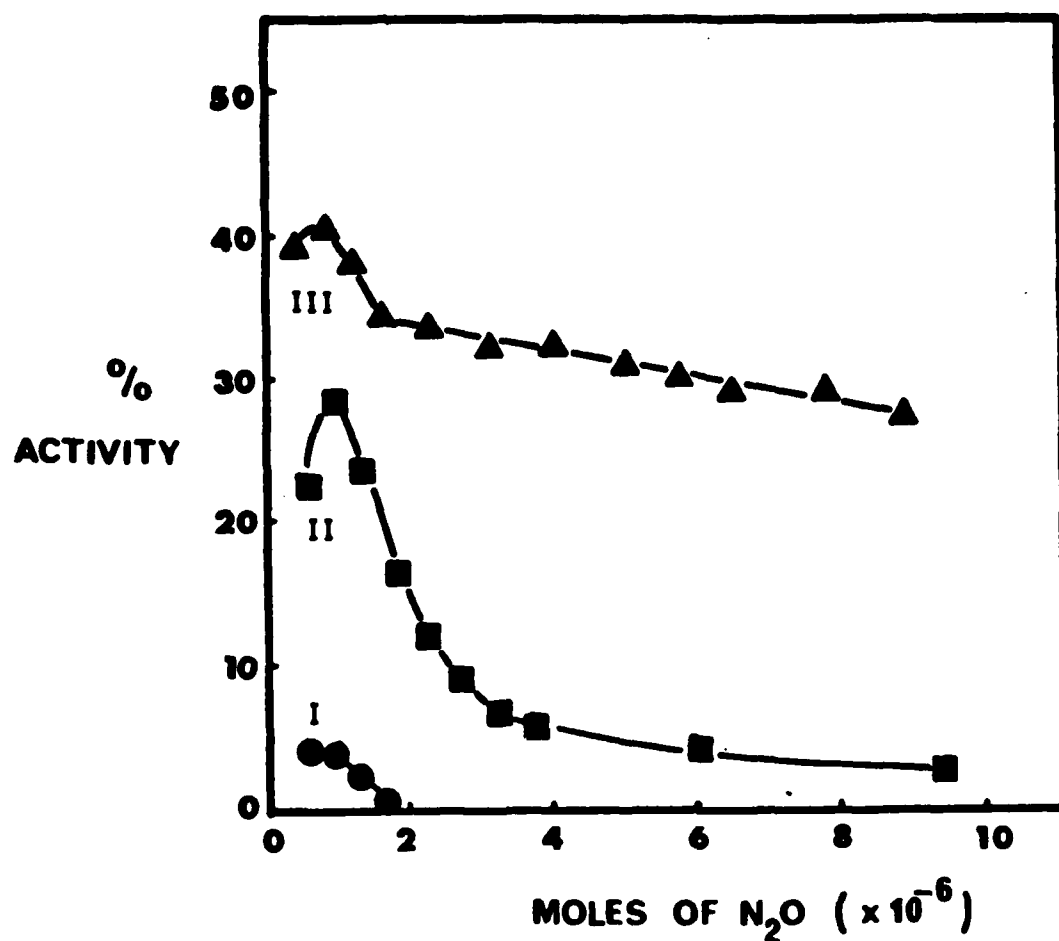
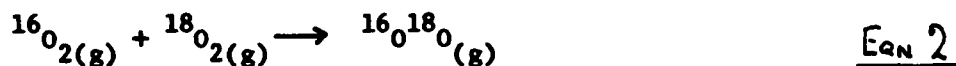


FIGURE A-7

PROFILES OF THE INITIAL ACTIVITY OF SrO AFTER PREACTIVATION AT THREE DIFFERENT TEMPERATURES FOR THE CONVERSION, $N_2O \rightarrow N_2 + xO_2$, AT 758 K. EACH DATA POINT REPRESENTS % CONVERSION TO N_2 OBSERVED FOR INDIVIDUAL PULSE FROM THE FIRST PULSE UPWARD. EACH PULSE $\sim 4 \times 10^{-7}$ MOLES OF N_2O AND THE BOTTOM AXIS IS THE CUMULATIVE NUMBER OF MOLES OF N_2O INTRODUCED AT $P_{N_2O} = 40$ TORR IN THE PULSED MICROCATALYTIC G.C. PROCEDURE. PLOT (I), DATA POINTS \bullet = ACTIVATION AT 993 K; PLOT (II), DATA POINTS \blacksquare = ACTIVATION AT 1083 K; PLOT (III) DATA POINTS \blacktriangle = ACTIVATION AT 1273 K.

respectively.

Oxygen isotope exchange was studied using Mass Spectrometry. Over suitably preactivated SrO samples the reaction occurred readily at room temperature, as shown in Figure 8, where the mole fractions of $^{16}\text{O}_2$, $^{16}\text{O}^{18}\text{O}$ and $^{18}\text{O}_2$ viz X_{32} , X_{34} and X_{36} respectively are plotted as a function of time. During the course of the reaction the atom fraction of ^{16}O and ^{18}O remained constant in the gas phase, thus indicating that an R_0 -type isotopic exchange process was occurring, i.e.



but not an R_1 or R_2 -type process. However, the exchange data did not exactly obey reversible second-order kinetics, as was found previously for oxygen isotope over ZnO (21). The effect of activation temperature on the exchange activity is shown in Figure 6A plot(ii) where the reciprocal of the time taken to reach half the equilibrium composition (taken as a measure of the reaction rate) is plotted as a function of outgassing temperature. Comparing this plot with Figure 6A plot (i) shows that higher outgassing temperatures (1273 K) were needed to confer high activity for room temperature oxygen isotopic exchange process than for N_2O decomposition (1023K). It is also evident that a much sharper cut-off point exists between outgassing temperatures producing active or non-active surfaces for the exchange reaction.

DISCUSSION

A degree of consistency between certain aspects of foregoing results and existing hypotheses as to the central importance of cations and/or anions at surface sites of high co-ordinative unsatur-

SrO sample with a succession of individual pulses of nitrous oxide. In this way profiles of initial activity could be developed. Figure 7 shows how the initial activity varied with increasing pulse number (each pulse -4×10^{-7} mole of N_2O) for SrO activated at 3 different temperatures. Comparison of the three Initial Activity profiles, all measured at identical reactor temperatures, demonstrate two important points: firstly, the activity maximum attained in profile was lowest after preactivation in vacuo at 993K and was increased by increased preactivation temperature; and secondly that, although the drop-off in activity after the maximum was quite abrupt for sample preactivated at 993K or 1083K (so that activity declined rapidly towards zero after a small number of pulses) no such abrupt drop-off in activity was found for the sample preactivated at 1273K. Rather the activity for N_2O decomposition continued at a high level up to large pulse numbers when the sample had been preactivated at this high temperature. The first of these points agree well with the existing hypotheses that the level of surface activity depends upon the extent to which more highly coordinatively unsaturated surface ions are exposed/developed at progressively higher preactivation temperatures. An adequate explanation of the second point requires some extension/modification of existing hypothesis which is attempted in the Discussion. Such extension/modifications are also relevant to observations made upon the ratio of N_2 to O_2 products from N_2O pulses at the temperatures depicted in Fig. 7. These showed that whilst at any of the selected temperatures the N_2/O_2 product ratio did not vary with pulse number, the ratio took values of 2.0, 3.0 and 3.8 during sequences of pulses introduced are samples previously outgassed at 993, 1083 and 1273K

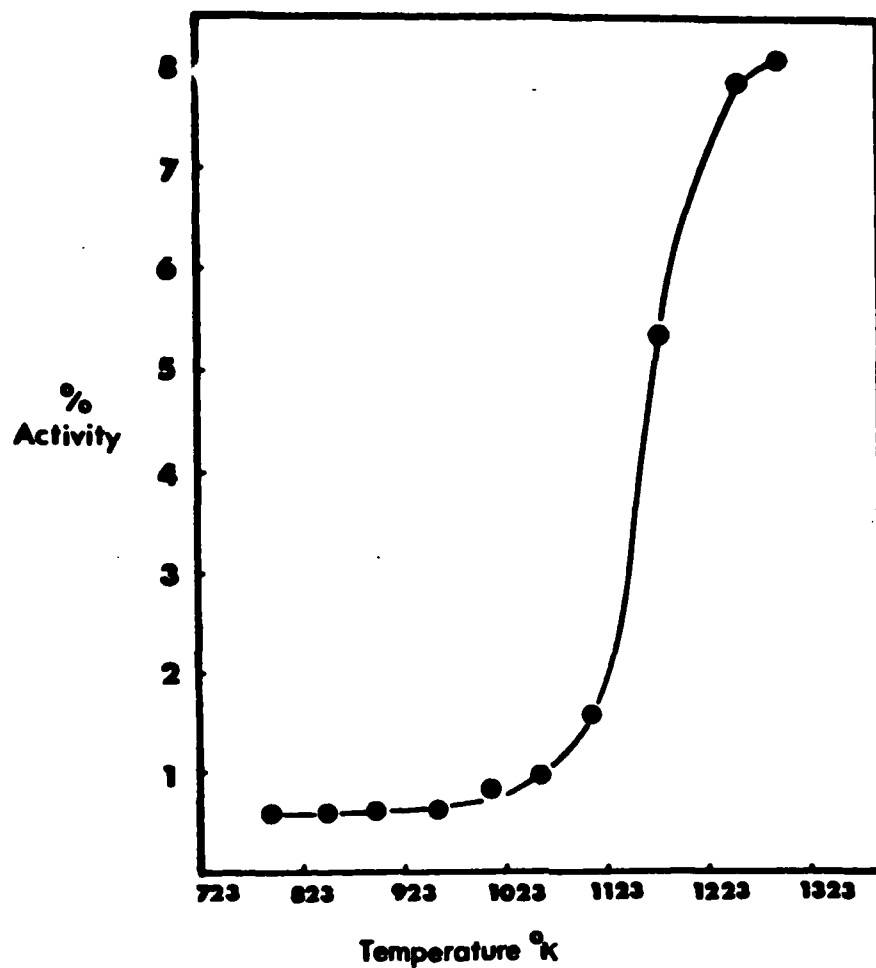


FIGURE A-6b

EFFECT OF PREACTIVATION TEMPERATURE (BOTTOM AXIS) UPON
 STEADY STATE ACTIVITY OF SrO FOR N_2O DECOMPOSITION AT
 758 K, AS OBSERVED BY CONTINUOUS-FLOW G.C. PROCEDURE WITH
 INPUT $P_{N_2O} = 380$ TORR.

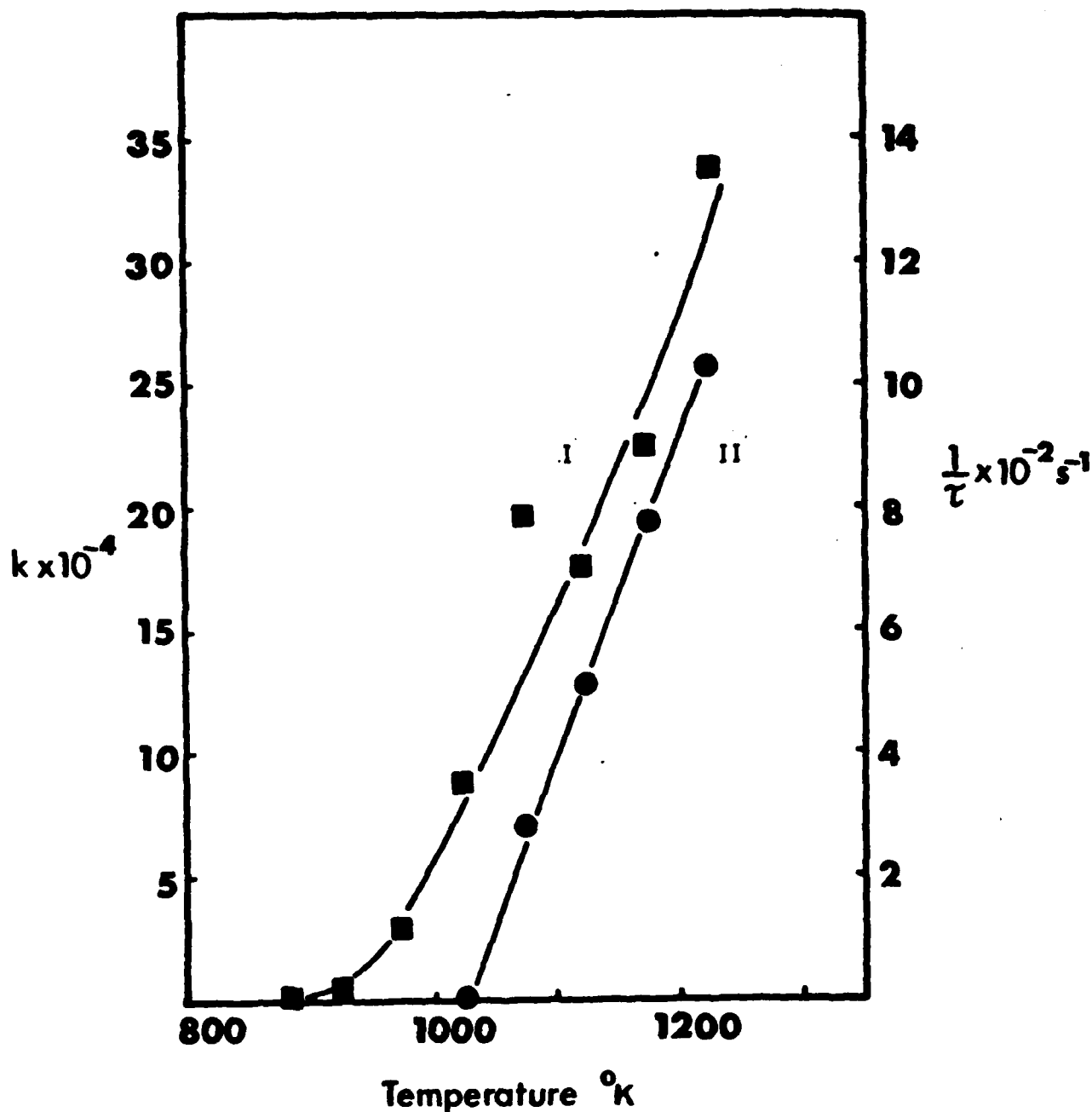


FIGURE 4-6a

EFFECT OF PREACTIVATION TEMPERATURE UPON KINETIC PARAMETERS FOR N_2O DECOMPOSITION AT 758 K (PLOT I, DATA POINTS ■) AND FOR OXYGEN ISOTOPE EXCHANGE AT 290 K OVER 50 MG OF SrO (PLOT II, DATA POINTS ●). THE KINETIC PARAMETER USED AS A MEASURE OF CATALYTIC ACTIVITY OF THE PREACTIVATED SAMPLE FOR DECOMPOSITION OF $\text{P}_{\text{N}_2\text{O}} = 2.5$ TORR WAS THE SLOPE OF PLOTS SIMILAR TO FIG. 4. FOR OXYGEN ISOTOPE EXCHANGE THE KINETIC PARAMETER UTILISED AS A MEASURE OF ACTIVITY WAS T_1 FOR ISOTOPIC EQUILIBRATION OF AN INITIAL PRESSURE OF 0.1 TORR OF ($^{16}\text{O}_2 + ^{18}\text{O}_2$) (CF. FIG. 8).

pressures through saturation of a small surface concentration of Sr_{4c}^{2+} , and our observation of accurate first order dependence upon $P_{\text{N}_2\text{O}}$ up to high pressures (cf. Fig. 5b), makes it probable that 5c rather than 5b was the r.d.p. in the continuous-flow conditions.

Typical net exposures of a preactivated SrO to nitrous oxide in the mass spectrometric procedure ($\sim 6 \times 10^3$ torr sec) were intermediate between those in the pulsed g.c. procedure (40 torr sec per pulse) and in the continuous-flow g.c. procedure ($1 - 5 \times 10^6$ torr sec). Consistency with foregoing discussion would thus point to the possibility for contributions not only by anionic diffusion into the bulk but also by process 5 to the effective regeneration of Sr_{4c}^{2+} sites. The latter is implied by our mass spectrometric observation (cf. Fig. 4) of pseudo first order kinetics in the decomposition of $P_{\text{N}_2\text{O}} \sim 2.5$ torr in a static reactor. However our hopes that these mass spectrometric results would provide further insight into the relative importance of various regenerative steps were not realised, partly because of instrumental difficulties which made the ratio between N_2 and O_2 product subject to some uncertainty. Furthermore, Winter had demonstrated (29) that adherence to the pseudo first-order kinetics in the decomposition of N_2O to ca. 50% reaction over metal oxides was not a sufficient criterion for determining if removal of oxygen to the gas phase had an important rate determining role.

Evidence for an important role of coordinatively unsaturated metal ions has been given in published work from these laboratories (29-31) upon R_O -type oxygen isotope exchange (cf. eqn. 2) at room temperature over preactivated surfaces of ZnO , Tl_2O_3 or MgO . Recognition was also given to a need for the availability of a very weakly held electron in

the proximity of M_{CUS}^{2+} , in order for the active site to be able to trigger R_{O} -type oxygen isotope exchange by an electron transfer-catalysed chain process requiring negligible energy of activation. Both of these requirements seem likely to be satisfied by the $(O_{\text{LC}}^{2-} \dots F_{\text{S}}^{+})$ surface locations proposed by Duley (5a) as being responsible for surface luminescence from high surface area MgO and CaO, since: (a) the Sr^{2+} cations involved in the F_{S}^{+} point defect necessarily have at least two degrees of co-ordination unsaturation, and (b) relatively low energies can be expected for transfer of an electron from a ground state O_{LC}^{2-} to an adjacent F_{S}^{+} . Thus, according to Duley's interpretation such transfer is responsible for a broad absorption centered upon 2 eV and detectable in MgO previously exposed to high energy radiations in vacuo. Still lower energy could be expected for thermal, rather than optical, promotion of an electron from O_{LC}^{2-} to an adjacent F_{S}^{+} for MgO. Further reductions in energy could be anticipated for SrO relative to MgO, and for $(O_{\text{C}}^{2-} \dots F_{\text{S}}^{+})$ locations relative to $(O_{\text{LC}}^{2-} \dots F_{\text{S}}^{+})$. Thus it is reasonable to envisage o.i.e. upon SrO proceeding, in analagous fashion to that previously detected for ZnO surfaces, via activation of oxygen under the combined influence of a readily available electron and coordinatively unsaturated cation(s). Viewed in this context the experimentally observed dependence of the extent of room-temperature o.i.e. activity of the SrO (ex SrCO_3) surfaces upon temperature of prior activation (cf. plot ii of Fig. 9), should reflect the increase in number of $(O_{\text{LC}}^{2-} \dots F_{\text{S}}^{n+})$ surface locations with preactivation temperature ($n = 1$ or 2).

Our observation that appreciable room temperature oxygen isotope exchange activity only appeared after preactivation at ≥ 1023 K (cf. plot (ii) of Fig. 6A) correlates particularly well with the Fig. 6B showing a similar dependence upon preactivation temperature in the emergence of catalytic activity for sustained steady state decomposition of N_2O . As commonly envisaged, the mechanisms of each catalysed process involves reversible electron transfer/sharing between metal oxide surface and adsorbate-related surface species. The good correlation observed between their requisite preactivation temperatures probably reflects their common requirement for reversible electron transfer with the SrO surface. The emergence of some limited surface-assisted N_2O decomposition after somewhat less rigorous surface preactivation (e.g. at 973 K in plot (i) of Fig. 6A, or 993 K in plot (i) of Fig. 7) may, on the other hand, reflect a small extent of irreversible electron transfer to N_2O .

Acknowledgements

This work was supported by the U.S. Air Force Office of Scientific Research under grants AFOSR 82-0023 and 83-0074. Experimental facilities for the luminescence measurements were made available at Harwell Atomic Energy Establishment

through the courtesy of the late Dr. A.J. Tench. The authors are also grateful to Professor F. Stone and Dr. Wm. Mackrodt for stimulating discussions.

REFERENCES (cited in Appendix A)

1. (a) J.E. Ely, K.J. Teegarden and D.B. Dutton, *Phys.Rev.*, (1959), 116, 1099.
2. (a) D.L. Dexter and R.S. Knox, *Excitons*, Int rscience Publishers, 1965;
(b) T. Higashimura, Y. Nukaoka and T. Iida, *J.Phys.C.Solid State Phys.*, 1984, 17, 4127.
3. B. Henderson and J.E. Wertz, *Adv.Physics*, 1978, 17, 749.
4. V.M. Bermudez, *Prog.Surf.Sci.*, 1981, 11, 1.
5. (a) W.W. Duley, *Phil.Mag.B.*, 1984, 49, 159; (b) K. Teegarden in *Luminescence of Inorganic Solids*, ed. P. Goldberg, Academic Press, New York, 1966.
6. R.C. Whitel and W.C. Walker, *Phys.Rev.*, 1969, 188, 1380.
7. A. Zecchina, M.G. Lofthouse and F.S. Stone, *J.Chem.Soc.Faraday Trans I*, 1975, 71, 1476.
8. E. Garrone, A. Zecchina and F.S. Stone, *Phil.Mag*, 1980, B42, 683.
9. A.J. Tench and G.T. Pott, *Chem.Phys.Lett.*, 1974, 26, 59a;
10. S. Colluccia, A.M. Deane, A.J. Tench, *J.Chem.Soc.Faraday Trans I*, 1978, 74, 2913.
11. S. Colluccia, and A.J. Tench, *J.Chem.Soc.Faraday Trans I*, 1983, 79, 1881.
12. E.A. Colbourn, J. Kendrick and W.C. Mackrodt, *Surface Science*, 1983, 126, 550.
13. V.M. Bermudez, *Prog.Surf.Science*, 1981, 11, 1.
14. W.H. Hamill, *Phys.Rev.*, 1969, 185, 1182.
15. D. Cordischi, V. Indovina and M. Occhiuzzi, *J.Chem.Soc.Faraday Trans I*, 1978, 74, 456; (b) V. Indovina and D. Cordischi, *loc.cit.*, 1982, 78, 1705.
16. M.J. Baird and J.H. Lunsford, *J.Catal.*, 1972, 26, 440;
(b) Y. Tanaka, H. Hattori and K. Tanaka, *Chem.Lett.*, 1976, 37.
17. (a) H. Hattori and A. Satch, *J.Catal.*, 1976, 45, 32;
(b) M. Mohri, K. Tanabe and H. Hattori, *J.Catal.*, 1974, 33, 144.
18. (a) H. Hattori, K. Marayama and K. Tanabe, *J.Catal.*, 1976, 44, 50;
(b) M. Mohri, H. Hattori and K. Tanabe, *J.Catal.*, 1974, 32, 144.
19. (a) L. Parrot, J.W. Rogers, Jr., and J.M. White, *Appl.Surf.Ser.*, 1978, 1, 443;
(b) H. Noeller and K. Thomke, *J.Mol.Catal.*, 1979, 6, 375.

20. J. Cunningham, B.K. Hodnett, M. Ilyas, J.P. Tobin and E.L. Leahy, *Faraday Discuss Chem.Soc.*, 1981, 72, 283.
21. K. Nakamoto, *Infrared and Raman Spectra of Inorganic and Coordination Compounds*, 3rd ed., Wiley Interscience, New York, 1978;
- (b) S. Pinchas and I. Ilalicht, *Infrared Spectra of Labelled Compounds*, Academic Press, 1971, p.
22. P.A. Tausker, E.A. Colbourn and W.C. Mackrodt, *J.Am.Ceramic Soc.*, (in press).
23. R.H. Milne, *Surface Science*, 1982, 121, 347.
24. C.J. Vempati and P.W.M. Jacobs, *Cryst.Lat.Def. and Amorph Mat.*, 1983, 10, 9.
25. S.P. Muraska and R.A. Swalin, *J.Phys.Chem.Solids*, 1971, 32, 1277 and 2015.
26. J. Cunningham, J.J. Kelly and A.L. Penny, *J.Chem.Soc.Faraday Trans I.*, (a) 1970, 74, 1992; (b) 1971, 75, 617.
27. N.B. Wong, Ben Taarit and J.H. Lunsford, *J.Chem.Phys.*, 1974, 60, 2149.
28. F.S. Stone, *J.Solid State Chem.*, 1975, 12, 271;
- (b) G. Blyholder, *J.Phys.Chem.*, 1971, 75, 1037.
29. E.R.S. Winter, *J.Catal.*, 1974, 34, 431.
30. J. Cunningham and E.L. Goold, *J.Chem.Soc.Faraday Trans I*, 1981, 77, 837; (b) J. Cunningham, E.L. Goold and J.L.G. Fields, *loc.cit.*, 1982, 78, 785.
31. J. Cunningham in *Comprehensive Chemical Kinetics*, vol. 19, (eds. C.F. Tipper and C.H. Bamford), Elsevier, Amsterdam, 1984, p. 362.

APPENDIX B

TITLE: SPECTROSCOPIC AND KINETIC STUDIES OF SURFACE PROCESSES ON ALKALINE
EARTH OXIDES. EFFECTS OF Ba^{2+} DOPANT UPON MgO

PAPER PRESENTED JUNE 1984

AT

BRUNEL UNIVERSITY

UXBRIDGE, MIDDLESEX UB8 3PH, UK

AT INTERNATIONAL SYMPOSIUM

ON

"ADSORPTION AND CATALYSIS ON OXIDE SURFACES"

SCHEDULED FOR PUBLICATION IN BOOK FORM BY ELSEVIER (1984)

SPECTROSCOPIC AND KINETIC STUDIES OF SURFACE PROCESSES ON ALKALINE EARTH OXIDES.

EFFECTS OF Ba^{2+} DOPANT UPON MgO

J. NUNAN¹, J. CUNNINGHAM¹, A.M. DEANE³, E.A. COLBOURN² and W.C. MACKRODT²

¹ Department of Chemistry, University College, Cork, Ireland

² I.C.I., New Science Group, Runcorn, Cheshire, England

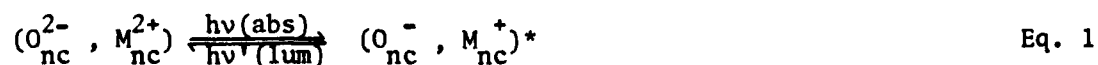
³ A.E.R.E., Harwell, Abingdon, England

ABSTRACT

Computations of the structural consequences of segregation of Ba^{2+} at monolayer and submonolayer coverages on (001) surfaces of MgO indicate extensive reconstruction. The predicted reconstruction for $\text{Ba}^{2+}/\text{MgO}$ contrasts sharply with insignificant reconstruction reported for pure MgO surfaces. Results are described for experimental comparisons of the surface luminescence and surface reactivity of high surface area samples of $\text{Ba}^{2+}/\text{MgO}$ with MgO and BaO . Extent of agreement is assessed between the observed Ba^{2+} -related effects and these working hypotheses: (i) that the Ba^{2+} induces surface reconstruction of the type calculated, to yield surface anions and cations in positions of altered, but non-integral, co-ordination; (ii) that photoexcitation of electrons at such $\text{O}_{\text{cus}}^{2-}$ sites are responsible for enhanced luminescence; and (iii) that $\text{Ba}_{\text{cus}}^{2+}$ sites are involved in enhanced reactivity towards N_2O at 300 K.

INTRODUCTION

Luminescence and reactivity of surfaces of alkaline earth oxides are the particular facets of Tony Tench's distinguished and many-faceted contributions to the study of metal oxides which will primarily concern us in this paper. Thanks largely to the spectroscopic equipment and sample pretreatment procedures developed in Tony's laboratory (ref. 1-3), it became possible to attain and characterise reproducible spectroscopic parameters (cf. table 1) for the luminescence detectable from high surface area samples of alkaline earth oxides. The development of a conviction that extrinsic surface states were strongly implicated in this and other properties of high surface area ionic (h.s.a.i.) oxides soon became evident (ref. 4,5). Indeed, a confluence of such proposals by Tench and co-workers concerning surface luminescence with those from Stone and co-workers (ref. 6-9) concerning diffuse reflectance from h.s.a.i. oxides contributed to interpretation of these spectroscopic features in terms of surface-exciton (s.e.) models. As the name implies, such s.e. models recognise important differences between excitons at the surface (a correlated hole-electron pair produced at the surface by the absorption of an appropriate photon in the visible or near-uv) and those within the bulk. Equation 1 summarises one formalism adopted in the literature to allow distinction to be made between excitons on the basis of differences between the extent of co-ordination (or conversely the extent of co-ordinative unsaturation) of the ion sites involved. Subscripts nc in this



equation denotes the degree of co-ordinative saturation of the lattice oxygen anion from which (in the one-excited electron approximation) an electron is

excited upon absorption of a photon, or to which it returns in radiative decay of an exciton. Within the bulk, $n = 6$ at regular lattice sites, whereas n is reduced to 5 with concomitant decrease in Madelung potential for ions at planar non-defective regions of (100) surfaces of MgO or other alkaline earth oxides. Further reductions of n to 4 at surface defect locations (such as an edge or step upon the (100) surface), or to 3 at a defect site of high coordinative unsaturation (such as a corner or kink site), have also been envisaged. Satisfactory agreement has been reported by Stone (ref. 9) between transition energies calculated for $h\nu(\text{abs})$ of Eq. 1, on the basis of static Madelung potentials appropriate to $n = 5, 4$ & 3 , and features (usually three in number) partially resolved in the diffuse reflectance spectra of MgO, CaO, SrO and BaO. It is worth noting the relatively large magnitude of the red-shifts, e.g. up to 3.5 eV in the case of MgO, which these calculations seek to account for in terms of differences in static Madelung potential envisaged for $\text{O}_{\text{nc}}^{2-}$ having $n = 6, 5, 4$ or 3 . Results of some recent experiments and computations have called into question the wisdom/validity of seeking thus to account for such large red-shifts mainly in terms of diminished static Madelung potential at surface defect locations whereon n takes the integral values of 3, 4 or 5. Computations have been made with models which simulate defective non-planar surface regions whereon some surface ions are initially positioned at corner/kink sites for which n would nominally be 3, and some at edge/step sites for which $n = 4$ (ref. 10). Such computations indicate that, in marked contrast to ions having $n = 5$ at flat non-defect terraces (ref. 10), ions at surface defect positions may experience large relaxation, e.g. up to 0.45 \AA inward for $\text{O}_{4\text{c}}^{2-}$ in its ground electronic state. The accuracy of earlier calculations which ignored such relaxation - as was implicit in their use of static Madelung potential and their restriction of n to the integers 3, 4 or 5 - may be questioned on this basis. Another incompletely resolved question

is the possibility that surface impurities/adsorbates located in the immediate proximity of surface O_{nc}^{2-} may influence the transition energy and/or probability for the optical transitions in eqn. 1, e.g., very recent reinvestigation of the luminescence from h.s.a.i. MgO points to the involvement of surface hydroxyls (ref. 11) in photoexcitation at 270 nm.

EXPERIMENTAL

Approach

The unresolved questions detailed in the introduction have here been addressed by a combination of: (a) computations aimed at predicting the effect of a surface impurity viz. Ba^{2+} , upon the structure of (001) faces of MgO and (b) experimental determination of the influence of Ba^{2+} surface dopant upon surface luminescence and surface reactivity of h.s.a.i. MgO. Details of the computational approach are given elsewhere in detail (ref. 12).

Materials

Steps for incorporation of Ba^{2+} dopant onto MgO consisted of adding 5 g of $Mg(OH)_2$ to aqueous $Ba(NO_3)_2$ containing the desired number of moles of Ba^{2+} , heating first to dryness and then at 600 K to convert $Mg(OH)_2$ to MgO and finally at 780 K to decompose $Ba(NO_3)_2$ to BaO. Evolution of gases at these various stages was monitored by mass spectrometry (Vacuum Generators Micromass 6), and also during subsequent activation of the material in vacuo while the temperature was increased stepwise from 780 to 1273 K. Two considerations made it highly unlikely that Ba^{2+} would migrate significantly into the lattice of the supporting oxide during such preparations: Firstly, the results of recent computations (ref. 12) showing that Ba^{2+} should have a strong tendency to segregate to the surface of MgO, CaO or SrO; and secondly, large energies, ca. 5 eV, for diffusion of cations via cation vacancy or interstitial mechanisms

TABLE 1

PARAMETERS OF OBSERVED SURFACE LUMINESCENCE FROM Ba^{2+} -DOPED MgO and RELEVANT
PROPERTIES OF MgO and BaO

Nominal surface loading by Ba^{2+} /monolayer equiv.	Luminescence Parameters		Surface Area $\text{m}^2 \text{g}^{-1}$	$\text{I}(\text{Ba}^{2+}/\text{MgO}) @ 460 \text{ nm}$ $\text{I}(\text{MgO}) @ 394 \text{ nm}$	
	Excitation	Emission			
	λ max	λ max			**
3.2 m.e. $\text{Ba}^{2+}/\text{MgO}$	280(vs)* 340(vs)	→ 460(vs) → 460(vs)	58		~ 10
1.6 m.e. $\text{Ba}^{2+}/\text{MgO}$	280(s) 335(s)	→ 456(s) → 456(s)			~ 15
0.6 m.e. $\text{Ba}^{2+}/\text{MgO}$	280(s) 330(s)	→ 452(vs) → 452(vs)			~ 20
0.3 m.e. $\text{Ba}^{2+}/\text{MgO}$	278(s) 330(w)	→ 416(m) → 450(w)			~ 5
0.06 m.e. $\text{Ba}^{2+}/\text{MgO}$	270(s)	→ 394(s)			~ 1
undoped MgO	270(s)	→ 394(s)	92		1.0
undoped BaO	280(vw)	→ 460(vw)	4.9		~ 10^{-2}

* Notations (vs), (m), (vw), etc., denote whether the luminescence feature was very strong, moderate or very weak, etc.

** Heading of the last column refers to the intensity ratio of emission at indicated wavelengths.

(ref. 13). The loadings of the host oxides with Ba^{2+} achieved by these procedures are, therefore, better expressed as monolayer equivalents (m.e.) than as mole percent relative to the weight of the support. The surface areas used in estimating the coverage as m.e. are listed in Table 1 and were determined at the CSIC Institute of Catalysis Madrid (courtesy of Dr. J.G. Fierro).

These estimated values of m.e. should be regarded as upper limits since some evidence for small microcrystallites of BaO (i.e. existing as other than monolayer dispersions) was found by transmission electron microscopy (courtesy of Madame Leclerq, CNRS, Institute of Catalysis, Lyon) for a sample of Ba²⁺/MgO with nominal loading of 3.2 m.e.

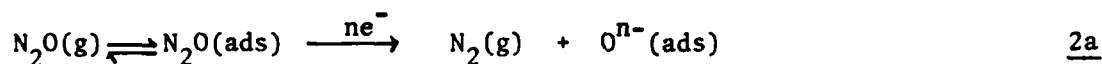
Spectroscopic Measurements

Preconditioning of the powdered samples in vacuo for 4 hours at 1273 K, whilst protected by liquid - N₂-cooled traps, was carried out in quartz sample holders prior to observations of their luminescence or diffuse reflectance spectra under front-surface illumination. Each holder had a rectangular section with parallel flat faces 2-3 mm apart into which the powders usually were shaken after preactivation and seal-off at the background pressure, ca.10⁻⁶, torr of the conventional vacuum system. When effects upon luminescence by the addition and/or removal of gases were to be determined, the sample of oxide was preactivated in situ within the rectangular section whilst remaining attached to a vacuum system at the spectrometer. The instrumentation used in obtaining the excitation/emission spectra has previously been described in detail (3). Excitation was provided by a 250 W Xenon lamp from which appropriate wavelengths were sequentially selected using two coupled Spex 14 monochromators whilst taking excitation spectra. A single Spex monochromator placed between sample and detector was held at a fixed wavelength and augmented by appropriate cut-off filters in taking excitation spectra. Spectra were automatically corrected for variations in excitation intensity with time or changing wavelength via instrumental comparisons (with an Ortec photon-counting system) of the pulse rates from two monochromators, one monitoring luminescence intensity and the other the intensity of the source at the same wavelength. Excitation spectra at acceptable signal/noise ratio were only obtained upward from 230 nm,

due to low source intensity at shorter wavelengths. Sharp cut-off filters (Corning 3-74 and O-52) were placed between the sample and the emission monochromator to minimise scattered wavelengths from the xenon source reaching the photomultiplier. A band-pass of 5 nm was used for both the excitation and emission results.

Measurement of Surface Reactivity

Largely on the basis of published evidence (ref. 14,15) that co-ordinatively unsaturated cations act as active sites for each process on other oxides, the gaseous conversions used to assess reactivity of the surface at 300 K after vacuum preactivation at selected temperatures were as follows:



and



Progress of each conversion was monitored by mass spectrometric analysis of gas samples taken at intervals from a static reactor following admittance of pure nitrous oxide or (50% $^{16}\text{O}_2$ + 50% $^{18}\text{O}_2$) at 300 K.

RESULTS AND INTERPRETATION

Computations

Figure 1 summarises results of computations indicating large reconstruction ('rumpling') effects of (100) surfaces of MgO whenever high concentration of Ba^{2+} are heavily segregated to the surface (i.e. approaching monolayer coverage by Ba^{2+}). In relation to $\text{Ba}^{2+}/\text{MgO}$ the following predictions should particularly be noted from this figure: (i) that all surface anions, O_s^{2-} , experience an outward displacement by 0.79 lattice units; (ii) that the

surface entity experiencing the greatest outward displacement - and hence the greatest degree of co-ordinative unsaturation - is that sub-set of surface cations, $\text{Ba}_{\text{cus}}^{2+}$, displaced by 1.21 lattice units; (iii) that the remaining 50% of surface Ba_s^{2+} experience a relatively small displacement by 0.38.

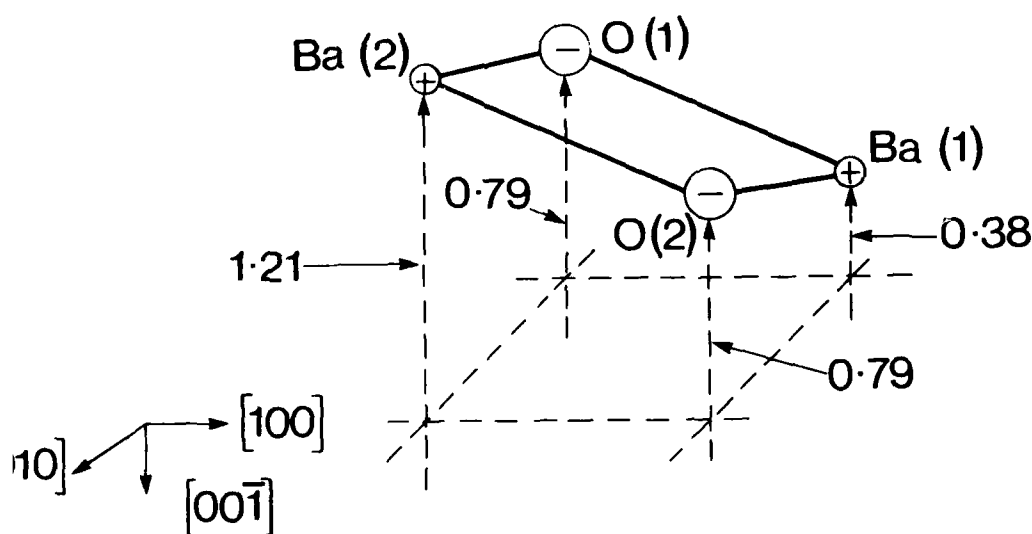
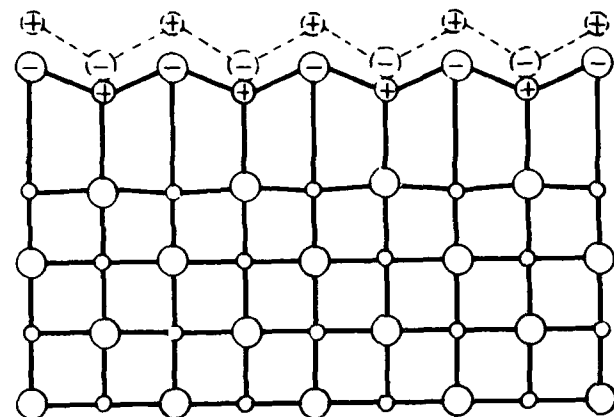


Fig.B1. Results of computations showing the reconstruction ('rumpling') of MgO surfaces having Ba^{2+} heavily segregated (to monolayer equivalent) to the surface. Numbers indicate (in lattice units) the outward displacement of two Ba^{2+} and two O^{2-} representing a unit cell of the reconstructed surface.

APPENDIX C

Results of AES and Work Function Measurements made by John Nunan,
J. Cunningham and John Tobin (deceased) upon $\text{Ba}^0/\text{SrO}/\text{Ni}$ and
 $\text{Ba}^0/\text{BaO}/\text{Ni}$ systems at Materials Laboratory, Wright Patterson Air force
Base - 14 March - 16 April, 1983 with the kind cooperation of the
Research Group of T.W. Haas, AFWAL.

The results on $\text{Ba}^0/\text{SrO}/\text{Ni}$ system, together with improved results for the
 $\text{Ba}^0/\text{BaO}/\text{Ni}$ system obtained by the research group of T.W. Haas, have been
submitted as a paper to the Fourth Cathode Workshop.

15. (b) J. Cunningham and E.L. Goold
J. Chem. Soc. Faraday Trans., 77 (1981) 837.
16. M. Che, A.J. Tench, S. Coluccia and A. Zecchina
J. Chem. Soc. Faraday Trans. I, 72 (1976) 1553.

REFERENCES (cited in Appendix B)

1. S. Coluccia, A.M. Deane and A.J. Tench
(a) J. Chem. Soc. Faraday Trans. I, 74 (1978) 2913.
(b) Proc. 6th Int. Cong. on Catalysis, London, 1976.
2. S. Coluccia, R.L. Segall and A.J. Tench
J. Chem. Soc. Faraday Trans. I, 75 (1979) 1769.
3. S. Coluccia and A.J. Tench
Proc. 7th Int. Cong. on Catalysis, Tokyo, 1980.
4. S. Coluccia and A.J. Tench
J. Chem. Soc. Faraday Trans. I, 79 (1983) 1881.
5. S. Coluccia, A. Barton and A.J. Tench
J. Chem. Soc. Faraday Trans. I, 77 (1981) 2203.
6. M. Che and A.J. Tench
Advances in Catalysis, 32 (1983) 1.
7. A. Zecchina, M.G. Lofthouse and F.S. Stone
J. Chem. Soc. Faraday Trans. I, 71 (1975) 1476.
8. A. Zecchina, M.G. Lofthouse and F.S. Stone
J. Chem. Soc. Faraday Trans. I, 72 (1976) 2364.
9. E. Garrone, A. Zecchina and F.S. Stone
Phil. Mag., 42 (1980) 683.
10. E.A. Colburn, J. Kendrick and W.C. Mackrodt
Surface Science, 126 (1983) 550.
11. W.J. Daley
J. Chem. Soc. Faraday Trans. I, 80 (1984) 1173.
12. (a) W.C. Mackrodt and R.F. Stewart
J. Phys., C12 (1979) 431.
(b) C.R.A. Catlow and W.C. Mackrodt
in Computer Simulation of Solids (Eds. Catlow and W.C. Mackrodt) Springer, Berlin, 1982.
(c) P.A. Tasker, E.A. Colburn and W.C. Mackrodt
J. Am. Ceramic Soc., (In Press).
13. C.S. Vempati, P.W.M. Jacobs
Cryst. Lat. and Amorph. Mat., 10, pp. 9-17 (1983).
14. J. Cunningham, J.J. Kelly and A.L. Penny
J. Phys. Chem.,
(a) 74 (1970) 1992.
(b) 75 (1971) 617.
15. (a) J. Cunningham, in C.H. Bamford and C.F. Tipper (eds.)
Comprehensive Chemical Kinetics, Vol. 19, ch. 3, Elsevier, Amsterdam, 1984.

activity appeared for e m.e. $\text{Ba}^{2+}/\text{MgO}$ following preactivation at only 900 K. Time to 50% equilibration of a 0.1 torr aliquot of ($^{16}\text{O}_2 + ^{18}\text{O}_2$) decreased to ca. 25 sec after preactivation at 993, 1053 or 1153 K but then increased again. Such dependence upon preactivation temperature for $\text{Ba}^{2+}/\text{MgO}$ contrasted with that noted for BaO and MgO but did resemble that found for N_2O dissociation over $\text{Ba}^{2+}/\text{MgO}$. That resemblance would, in the context of our working hypothesis for surface reconstruction, be explicable if the development of similar $\text{ne}^-/\text{Ba}_{\text{cus}}^{2+}$ surface locations by moderate preactivation were required to make possible both eqn. 2a and 2b and if such locations were diminished in number or subject to some deactivation upon outgassing at 1273 K.

ACKNOWLEDGMENTS

Spectroscopic aspects of this study were greatly facilitated through arrangements made by the late Dr. A.J. Tench for use of equipment at A.E.R.E. Harwell. The work was supported in part (J.N. and J.C.) through funding under AFOSR Contract 83-0074.

Evidence pointing to the importance of significant surface concentration of Ba^{2+} as a surface dopant, if activity for N_2O dissociation at 300 K was to be observable, came from comparisons of the activity of various samples subjected to identical preparation and preactivation in vacuo at 1273 K. These showed that, in marked contrast to $\text{Ba}^{2+}/\text{MgO}$ samples, neither undoped MgO nor BaO yielded detectable decomposition of N_2O at 300 K. Figure 5B illustrates some results of a comparison between the relative activities of $\text{Ba}^{2+}/\text{MgO}$ samples having different nominal loadings of Ba^{2+} . Maximum extent of decomposition was observed for the material with nominal loading of 1.5 m.e. which is close to where it could be expected on the basis of our working hypothesis, viz. at 1 m.e. when ca. 0.5 m.e. of $\text{Ba}_{\text{cus}}^{2+}$ displaced outward by 1.21 lattice units (cf. Fig. 1), and resulting high possibility for localization of excess electrons in the proximity of some $\text{Ba}_{\text{cus}}^{2+}$ sites, could be anticipated.

It was noted above that quenching of luminescence from $\text{Ba}^{2+}/\text{MgO}$ by oxygen was fully reversible and indicative of only weak interaction at the $\text{O}_2/\text{Ba}^{2+}/\text{MgO}$ interface. An electron-transfer initiated mechanism by which the R^{O} -type oxygen isotope exchange process of eqn. 2b can proceed at oxide surfaces via only weak interactions has been discussed elsewhere by one of the authors (ref. 15). That mechanism requires the availability of $\text{M}_{\text{cus}}^{2+}$ surface locations and it was of interest to determine experimentally whether, and after what preactivation temperature, eqn. 2b would be enhanced at $\text{O}_2/\text{Ba}^{2+}/\text{MgO}$ interfaces at 300 K. An enhancing effect of Ba^{2+} surface dopant was indeed found in respect of the relative room temperature activities of similarly preactivated samples of $\text{Ba}^{2+}/\text{MgO}$, MgO and BaO for the R^{O} -type oxygen isotope exchange process represented by eqn. 2b. Thus BaO surfaces developed significant activity only after outgassing for 6 h at 1293 K. Outgassing for at least 1 h at 1273 K was required to develop activity of the MgO material. However, appreciable

quenching by N_2O at 300 K to deactivation of some surface locations via irreversible N_2O dissociation thereon, as per the last step of eqn. 2a. It is important to recall from previous work that the availability of one or more excess electrons in the immediate vicinity has been recognised as a necessary, enabling feature of such decomposition sites (ref. 14). In respect of the observed reversible component of quenching by N_2O , present data do not suffice to determine whether this was mediated by $N_2O(ada)$, or $N_2O(g)$, or by both. Nor do they suffice to examine possible inter-relationships of P_{N_2O} with extent of decomposition and relative amounts of reversible and irreversible quenching.

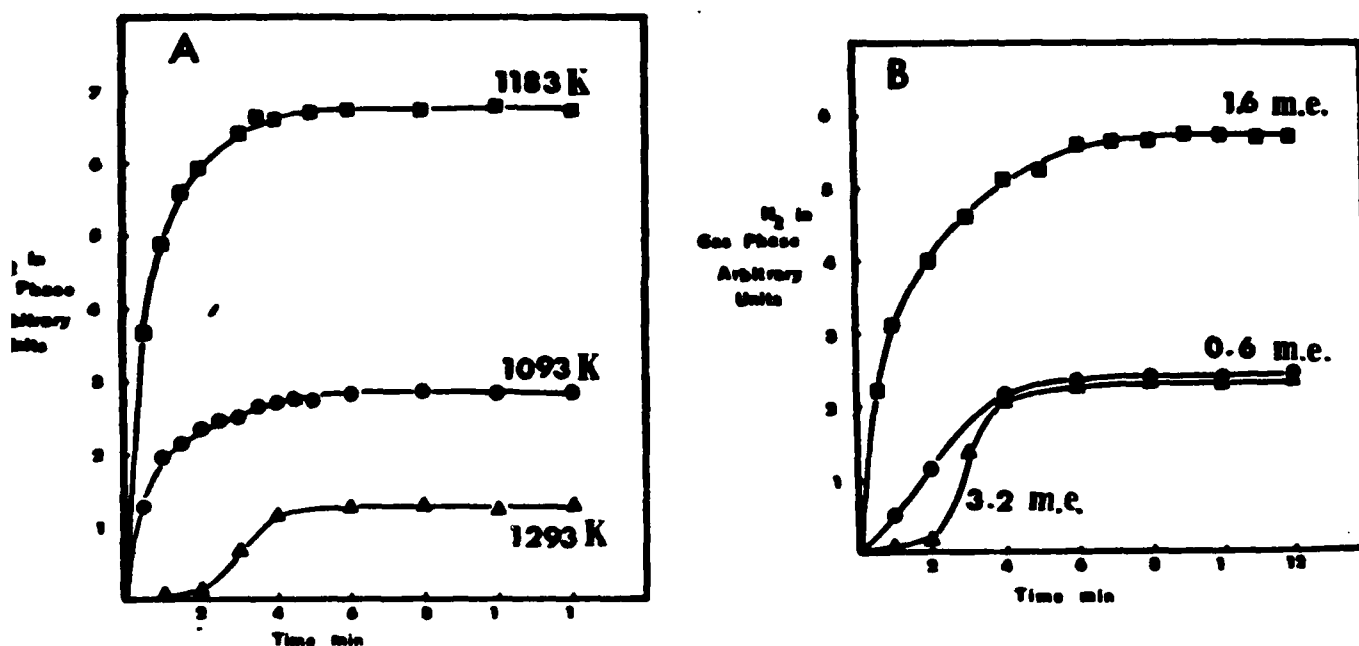
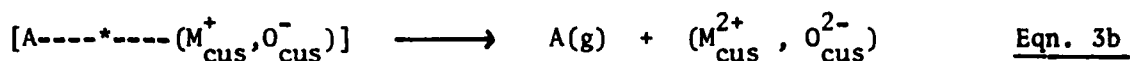
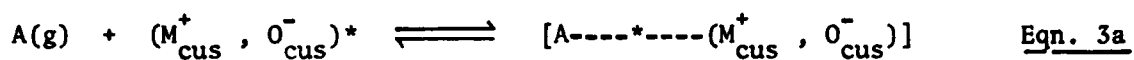


Figure B5. Build-up of N_2 product from N_2O dissociation at 300 K over Ba^{2+}/MgO samples in static reactor:

5A Relative rates of build-up over same 3.2 m.e. Ba^{2+}/MgO sample after preactivation at indicated temperatures.

5B Relative rates of build-up over different samples having indicated nominal surface loadings of Ba^{2+} . All samples similarly preactivated at 1273 K.



Quenching via such a charge-transfer-type exciplex avoids the need for significant complex formation in the ground state (recall difficulties reported in the literature in forming significant surface concentration of O_2^- on alkaline earth oxides ref. 16). Relative rate-coefficients for such electron-donor-acceptor type quenching by electron acceptors having differing electron affinities (e.a.) commonly decrease with decreasing e.a. However, our experimental observations showed the opposite to be the case, viz. that for any pressure in the range 10^{-2} to 10^{-1} torr, N_2O (e.a. ~ 0.1 eV) produced stronger quenching than O_2 (e.a. ~ 0.5 eV) at the same pressure (cf. Fig. 4B). This anomaly suggested that eqn. 3a and 3b on their own were not an adequate description of processes at the $N_2O/Ba^{2+}/MgO$ interface at 300 K. Subsequent paragraphs provide evidence of other interactions.

Surface Reactivity Studies at 300 K

Figure 5 demonstrates that samples of Ba^{2+}/MgO preactivated in vacuo at temperatures 1093-1293 K, i.e. in similar manner and across similar temperature range to that required for development of luminescence, retained an ability, after cooling to 300 K, to decompose carefully pre-purified N_2O , but to a rather limited extent. Maximum extent of this limited decomposition, is seen in Fig. 5A to have arisen after preactivation at 1183 rather than at 1093 or 1273 K, and corresponded to development of a partial pressure ca. 2×10^{-4} torr of N_2 in the static reactor. Since no O_2 product was detected in the gas phase and more N_2O was lost from the gas phase than the amount of N_2 detected, the observations were fully consistent with eqn. 2a. On that basis it seems reasonable to attribute the observed irreversible component in luminescence

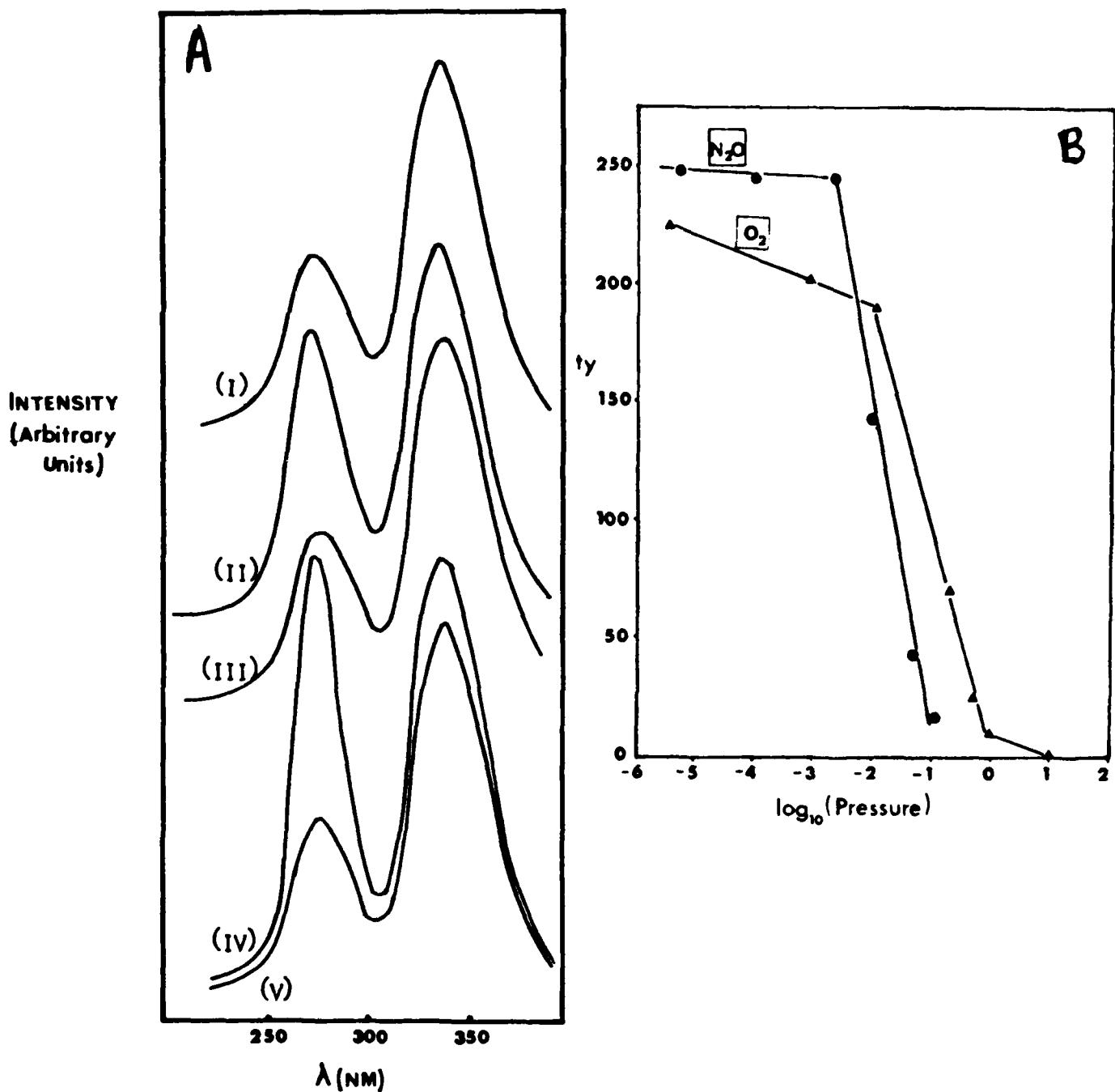


Figure B4. Effects of reducing gases (Part A) and oxidising gases (Part B) upon Ba^{2+} -related luminescence features of 3 m.e. $\text{Ba}^{2+}/\text{MgO}$:
4A photoexcitation spectra after: (I) enhanced outgassing; (II) contact with 10^{-2} torr H_2 ; (III) contact with 1 torr H_2 ; (IV) upon evac. of H_2 ; (V) after 3 h outgassing to 10^{-7} torr.
4B Extent of quenching of emission of 460 nm in the presence of indicated pressures of N_2O or O_2 at 300 K.

diminished a photoexcitation feature attributed to intrinsic excitations of OH^- ion in the $\text{Mg}(\text{OH})_2$ structure (ref. 11). Some final breakdown of surface $\text{Mg}(\text{OH})_2$ may have likewise contributed to the diminution of the photoexcitation feature at 277 nm in our prolonged outgassing of $\text{Ba}^{2+}/\text{MgO}$ at 1273 K. However, our observations that the introduction of H_2 at 300 K restored intensity to the photoexcitation feature at 277 nm and that this enhancement could be reversed by 2.5 h outgassing at 300 K (cf. Fig. 4) suggest an interesting alternative explanation, *viz.* that some H_2 released during breakdown of $\text{Mg}(\text{OH})_2$ remained as residual gas within the sample cell when sealed off in the routine outgassing procedure, whereas such residual gas was removed during the more rigorous outgassing procedure. A reversible enhancement of the 277 nm photoexcitation feature of $\text{Ba}^{2+}/\text{MgO}$ was also observed with introduction/removal of CH_4 . Reversibility at 300 K implies a weak interaction between the luminescence sites and H_2 or CH_4 , rather than a strong interaction such as dissociative chemisorption. Indeed our observation on the influence of H_2 and CH_4 on luminescence do not require any interaction with the ground state of the surface locations involved - only with their excited state.

Almost complete quenching of the Ba^{2+} -related luminescence features of $\text{Ba}^{2+}/\text{MgO}$ resulted when either of the oxidising gases O_2 or N_2O was present (cf. Fig 4B) at pressures ca. 1 torr. Evacuation of the gas at 300 K reversed this quenching almost totally for $\text{O}_2/\text{Ba}^{2+}/\text{MgO}$, but only partially (ca. 60%) in the case of $\text{N}_2\text{O}/\text{Ba}^{2+}/\text{MgO}$. Following other workers, who observed a reversible quenching by O_2 at undoped MgO and CaO and attributed it to formation of a weak complex with the electronically excited surface locations (refs. 2,6), quenching may be understood as the result of competition between radiative decay of surface excitons (cf. eqn. 1) and their diversion, as follows, into non-radiative decay via exciplex formation with O_2 and N_2O as oxidising gases

Figure 3 thus lends support to the use of emission at 455 ± 10 nm and of excitation at 340 ± 10 nm - both features being of very low intensity - as spectroscopic indicators of electronic transitions occurring at environments similar to those provided by the surface of BaO. In the literature, the relatively low surface areas measured for BaO, and the assumed lower density of surface defects, have been given as reasons for the notably low intensity of such features (ref. 8). While present results are not in conflict with such interpretation, the great enhancements in intensity which we observe (at similar transition energies) from $\text{Ba}^{2+}/\text{MgO}$ point towards operation of another factor additional to surface area-increase and factor-of-10 proportionate increase in defect-related $\text{O}_{\text{nc}}^{2-}$. As envisaged in our working hypothesis, reconstruction of the $\text{Ba}^{2+}/\text{MgO}$ surfaces can be such an additional factor. This would not be inconsistent with the observed similarities in $\lambda_{(\text{max})}$ for excitation and emission from BaO and $\text{Ba}^{2+}/\text{MgO}$, since on both surfaces Ba^{2+} would be the nearest cation neighbours to the O_{cus}^- sites involved in transitions (cf. Fig. 1).

Effects of Gases upon Luminescence at 300 K

Convincing evidence that the sites involved in luminescence from heavily doped $\text{Ba}^{2+}/\text{MgO}$ (Ba^{2+} loading nominally 3.2 m.e.) were located predominantly at the surface came from observations upon the sensitivity of luminescence to (i) the gases H_2 , CH_4 , O_2 and N_2O , and (ii) the rigour with which residual gases were removed in the preparation and outgassing procedure. Thus the intensity of the Ba^{2+} -related excitation feature at 340 nm was five-fold greater than that at 277 nm for rigorously outgassed samples, unlike the rather similar integrated intensities of these two excitation features in samples given the routine outgassing pretreatment (cf. plot(i) of Fig. 4 with Fig. 2A). Daley very recently reported that prolonged outgassing of $\text{Mg}(\text{OH})_2$ powder at 1200 K

weak emission centred around 550 nm in Fig. 3B was traced to the silica walls of the sample holder. Figure 3A shows excitation spectra obtained at rather poor signal-to-noise ratio by monitoring emission at 450 ± 10 nm from the BaO samples. Two excitation bands may be discerned having $\lambda_{(\max)}$ at 275 ± 10 and 340 ± 10 nm. The latter coincides, within the appreciable experimental error, to $\lambda_{(\max)}$ for the excitation feature which was very strong for $\text{Ba}^{2+}/\text{MgO}$ samples (cf. Fig. 2A).

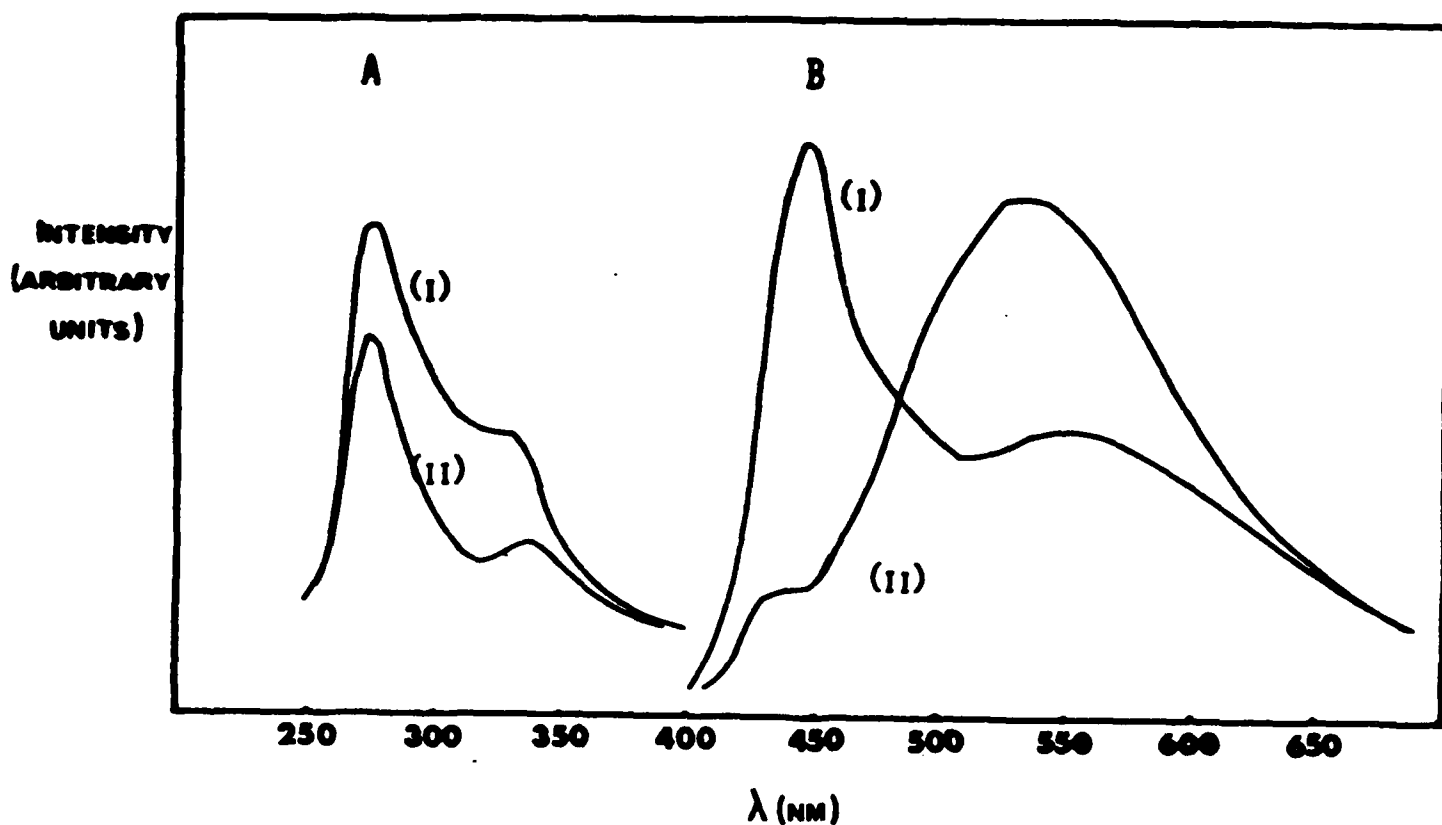


Figure B3. Excitation (Part A) and Emission (Part B) spectra at 293 K of unsupported BaO prepared from BaCO_3 and $\text{Ba}(\text{NO}_3)_2$; A(i) and (ii) respectively are excitation spectra of BaO prepared from BaCO_3 and $\text{Ba}(\text{NO}_3)_2$ monitored at emission wavelength = 460 nm; B(i) and (ii) are emission spectra of BaO, ex. BaCO_3 and $\text{Ba}(\text{NO}_3)_2$ respectively, excited at 335 nm.

dopant level exhibited by the intensity at 460 nm, $I(460)$, and by $\lambda_{(\max)}$ for the emission are summarised in Table 1. These demonstrate firstly that for Ba^{2+} loadings > 0.6 m.e., $\lambda_{(\max)}$ for emission remained at 456 ± 5 nm whether excited at 280 or 335 ± 5 nm and that $I(460)$ did not increase significantly with loading but rather declined slowly in this high-loading range. Secondly, the data for loadings < 0.6 m.e. show a precipitous drop in $I(460)$ with diminishing loading and a parallel displacement of $\lambda_{(\max)}$ away from 460 nm and back towards the $\lambda_{(\max)} = 416$ nm at 0.3 m.e. and $\lambda_{(\max)} = 394$ nm at 0.06 m.e. These results make it clear that only for loadings \ll monolayer did the emission of the support 'show through' clearly, whilst at moderate and high loadings the Ba^{2+} -related emission strongly predominated. In terms of the working hypothesis developed in an earlier paragraph this may be understood on the basis that, relative to a low surface density of defect-related $\text{O}_{\text{nc}}^{2-}$ locations upon non-reconstructed MgO surfaces, the Ba^{2+} -induced rumpling of the $\text{Ba}^{2+}/\text{MgO}$ surfaces caused a massive enhancement in the surface density of O_{s}^{2-} displaced into positions of diminished co-ordination (cf. Fig. 1A) and emitting at ca. 460 nm in analogous fashion to eqn. 1.

Preparation of h.s.a.i. BaO powder by thermal decomposition of BaCO_3 or $\text{Ba}(\text{NO}_3)_2$ was attempted with a view to comparing the luminescence parameters of the unsupported BaO with those just described for $\text{Ba}^{2+}/\text{MgO}$. Luminescence from the BaO preparations was, however, orders of magnitude less intense than from $\text{Ba}^{2+}/\text{MgO}$ samples, making it necessary to employ a 410 nm cut-off filter to diminish scattered/incompletely-monochromatised photons from the excitation source to flux levels comparable to any very weak luminescence at > 410 nm from the BaO samples. Emission spectra obtained in these conditions are shown in Fig. 3A, where a broad emission centred around 450 nm can be seen as well-developed for BaO ex- BaCO_3 but less well so for BaO ex- $\text{Ba}(\text{NO}_3)_2$. Only this emission feature seemed characteristic of BaO, since the broad and comparably

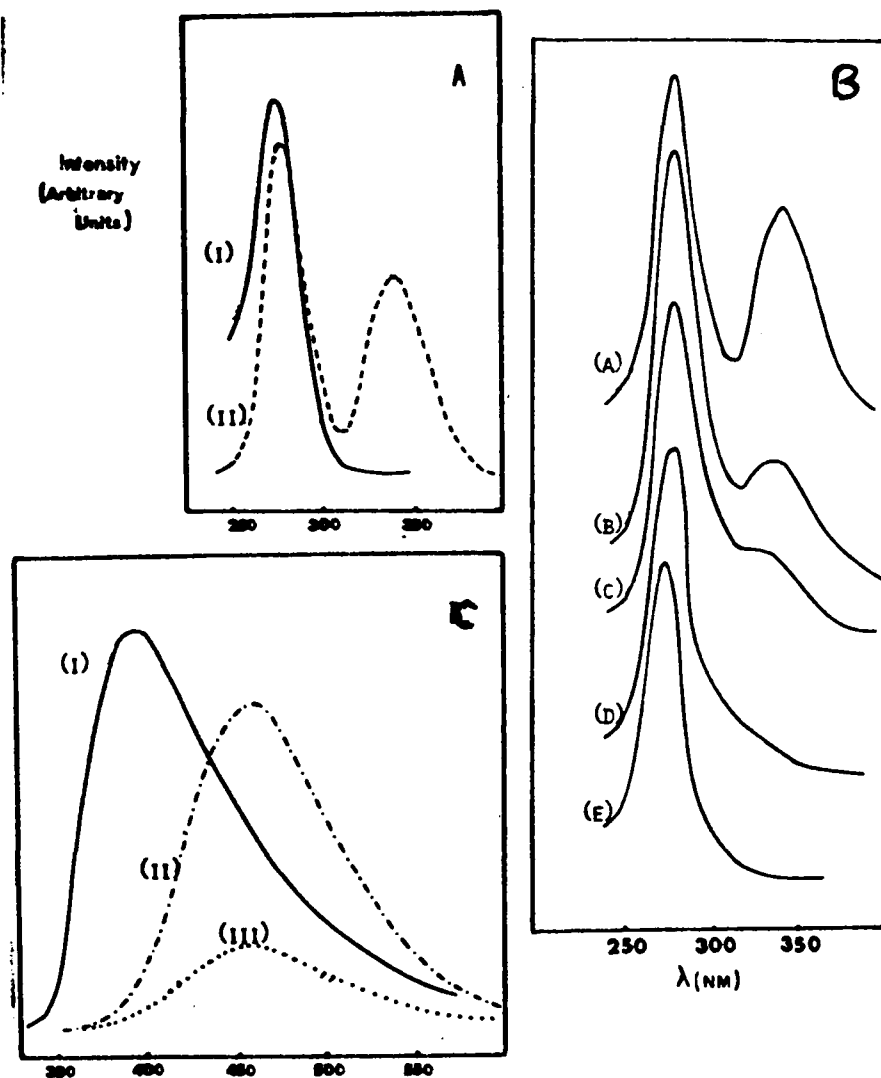


Figure B2. Effect of Ba^{2+} surface dopant upon photoexcitation, (Parts A and B), and luminescence/emission spectra, (Part C), relative to undoped MgO: 2A, Plot I, pure MgO, Plot II 3.2 m.e. $\text{Ba}^{2+}/\text{MgO}$; 2B Dependence of excitation features at 340 nm upon following nominal loading of MgO surface by Ba^{2+} - 3.2 m.e. (A), 1.6 m.e. (B), 0.6 m.e. (C), 0.3 m.e. (D) and 0.06 m.e. (E); 2C Differences in spectral distribution of emission from pure MgO (Plot I) and from 3.2 m.e. $\text{Ba}^{2+}/\text{MgO}$ excited at 340 nm (Plot II) or 280 nm (Plot III).

Spectroscopic Ba²⁺/MgO

Figure 2 demonstrates the striking changes brought about in the luminescence from MgO following incorporation of Ba²⁺ onto its surface. The excitation spectra shown in Part A of the figure show that, whereas undoped MgO gave rise to a single excitation band with $\lambda_{\max} \approx 270$ nm following preactivation of 1293 K in vacuo, (cf. plot A1), the Ba²⁺.MgO sample with a barium loading nominally equivalent to 3 m.e., gave two bands in its excitation spectrum with peaks at $\lambda_1 = 277$ and $\lambda_2 = 340$ nm respectively. Figure 2B illustrates the influence of decreasing the Ba²⁺-doping level upon excitation features for a series of Ba²⁺/MgO samples: — a rapid drop in the excitation feature of the MgO support should particularly be noted. This shows that the relative intensity of this excitation feature reflects the level of doping by Ba²⁺. A more complex situation, originating from overlap of the Ba²⁺ feature and those of the MgO support, clearly existed for the excitation feature with strong excitation intensities at 260-290 nm. The position of λ_{\max} for this feature was close to the 270 nm position characteristic of the MgO support. Assignment of the Ba²⁺-related excitation feature at 340 nm to luminescence as per eqn. 1, but involving surface O²⁻ displaced outward by 0.79 to positions of lower coordination, in the manner predicted by computations and summarised in Fig. 1, represented an attractive working hypothesis for explanation of the red-shift of λ_{\max} for this excitation. Evidence will emerge in the following paragraph that this working hypothesis can also help to account for greatly enhanced luminescence intensity from Ba²⁺/MgO relative to MgO or BaO. Plots of intensity of emitted luminescence versus wavelength of emission are compared for Ba²⁺/MgO and MgO in Fig. 2C. It may be noted that whereas MgO under excitation at 270 nm gave emission λ_{\max} at 395 nm, (cf. plot (i) of Fig. 2C), excitation of heavily doped Ba²⁺/MgO at either 280 or 340 nm (cf. plot(ii) of Fig. 2C). The results of preliminary studies of the dependence upon Ba²⁺

Experiments involved the controlled deposition in UHV conditions of zero-valent Ba^0 ad-atoms - in amounts ranging from submonolayer to multilayer coverage - upon layers of SrO or BaO previously prepared in UHV conditions by evaporation of the corresponding metal and its subsequent oxidation. These experiments related particularly to the important role widely envisaged for a thin coating of Ba^0 species upon oxide cathode surfaces in minimising their work-function under steady-state operation. Evaluation of work function changes with increasing coverage, θ_{Ba} , of the surface by Ba^0 thus represented the essential information sought from these studies of Ba^0 upon SrO and upon BaO layers. This information was derived from careful measurements of the electron energy distribution curve (EDC) for electron emission stimulated from the pure oxide and that covered with Ba^0 .

Auger electron spectroscopy was utilised to characterise the chemical composition/chemical purity of the evaporated layers. The most relevant AES spectra have been redrawn and are presented together in Figures 1 and 4 for comparison. All results presented are for the 4th nickel foil and for a sequence of measurements carried out in the last week of the stay in Dayton.

1. The Ba/SrO/Ni System: (Figures 1, 2 and 3)

Figure 1(a) is an AES spectrum of the nickel foil after repeated attempts to remove sulphur and carbon from the surface using argon ion bombardment. The following conditions were used: Argon pressure = 2×10^{-5} Torr ; $I = 5.0$ mA ; $V = 1.0$ k V.; Temperature of foil during ion bombardment = 980°C . Duration of ion bombardment = 10.0 mins. After ion bombardment the foil was heated to 1050°C for a further 10.0 minutes and the ion bombardment procedure repeated. The spectrum shown in Fig. 1(a) is of a sample taken through this procedure 8 times, the argon gas having been changed after the 6th cycle. The background pressure before ion bombardment was in the range of 1×10^{-9} Torr. (Ion bombardment with the nickel foil at room temperature was only effective in removing sulphur and oxygen, but not carbon). Heating with ion bombardment was effective in removing all three contaminants from the surface, but apparently also brought sulphur from the bulk to the surface, thus explaining the need for several cycles. All auger spectra were run in the scanning mode under the following instrument settings : $E_p = 2.4$ kV ; $V_{\text{Mode}} = 6$ eV ; R-C, 5×10^4 ms/ch. 40.0 in sec. ; $I_p = 100$ mA; $V_{\text{Mult}} = 2.0$ kV ; Sens. = 3.0 mV.

FIG. C-1

Auger spectra (a) nickel support after argon ion bombardment; (b) strontium deposited at $P = 2 \times 10^{-10} \text{ T}$ ($\theta_{\text{Sr}} = 16.0$), (c) oxidized at $P_{\text{O}_2} = 5 \times 10^{-7} \text{ T}$ 300°C for 1.0 h, and outgassed for 0.3 h. at 300°C ; (d) barium deposited on Ni/SrO ($\theta_{\text{Ba}} = 1.7$)

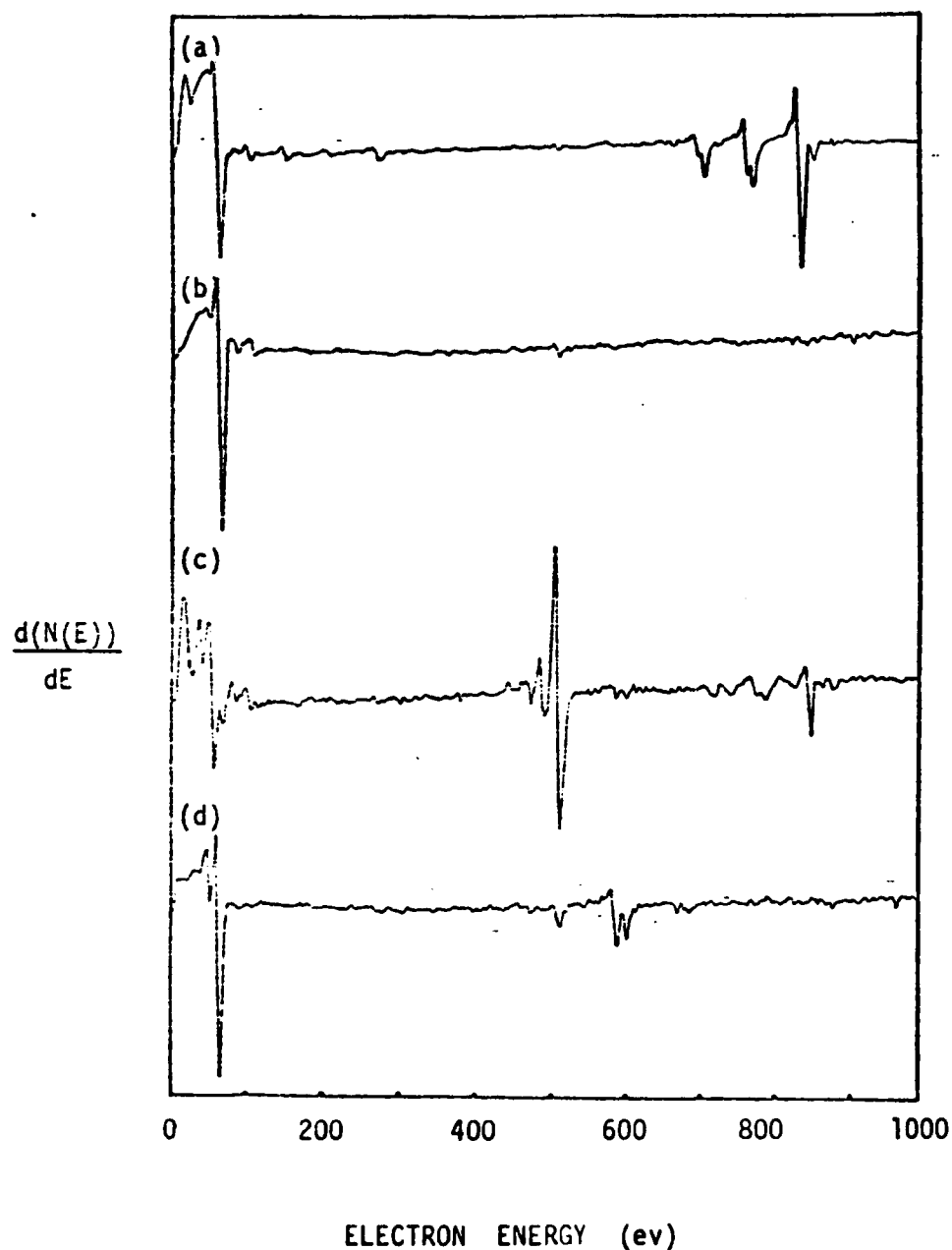
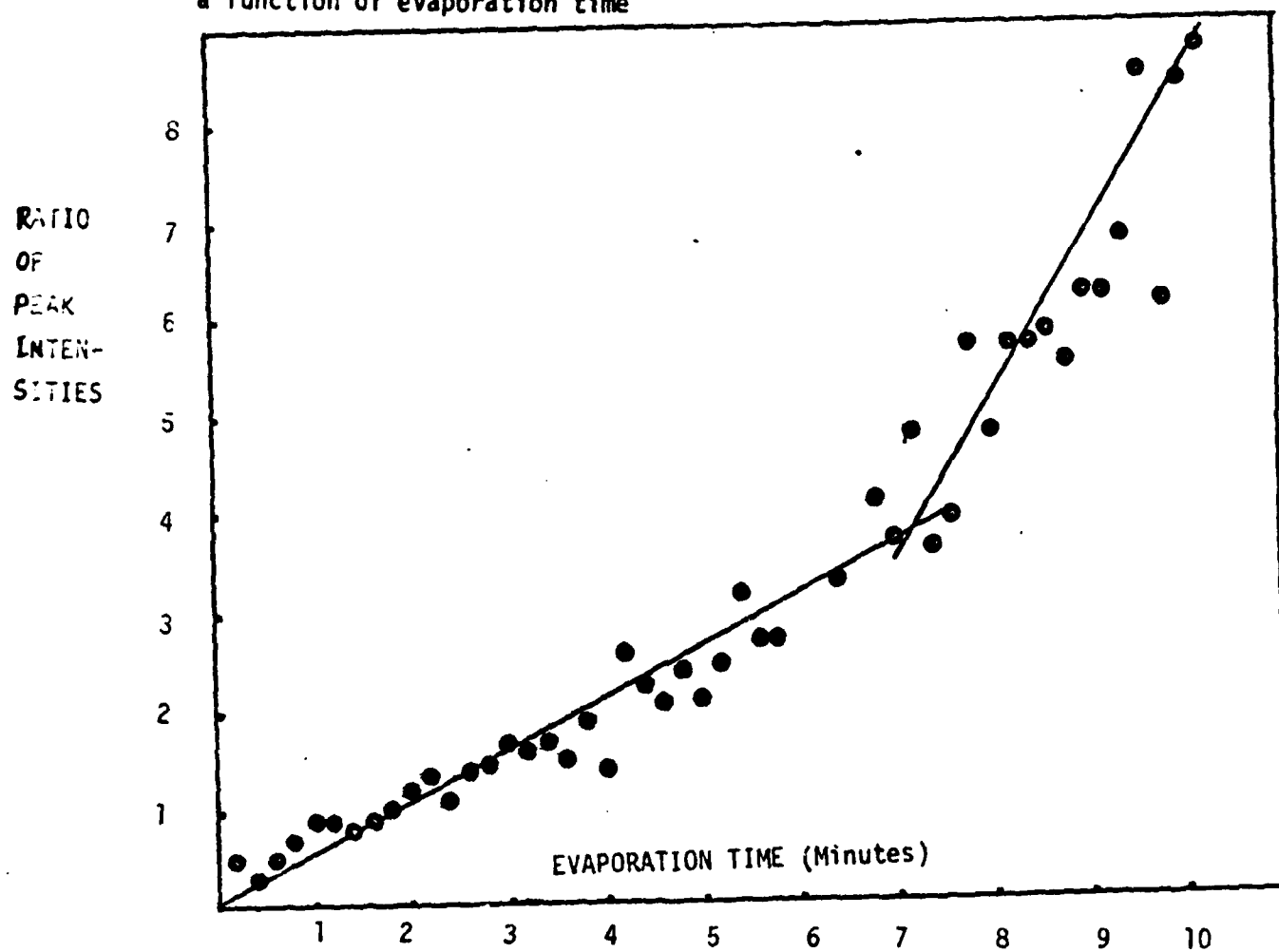


FIG.2-C: Ratio of the intensity of the strontium auger peak to the nickel peak as a function of evaporation time



In Figure 1(b) is shown the auger spectrum of the nickel foil after strontium evaporation for 2.0 hours with the current (I) of the evaporation set at 1.1 A. The background pressure was in the region of 2.0×10^{-10} Torr and spectrum 1b confirms coverage of the nickel by strontium metal with only a trace of oxygen. Figure 2 is a "break-point" plot derived from a series of SAES taken during deposition of strontium on nickel under the same evaporation conditions as used above. The change in slope evident at 7.3 min in Fig. 2 identifies this as the time for deposition of the first monolayer of strontium. It further indicates that the equivalent of sixteen layers of strontium were deposited on the nickel foil which resulted in Figure 1(b). This strontium multilayer was then exposed to oxygen at a pressure of 5×10^{-7} Torr for one hour whilst the nickel foil was heated by a current of 1.0 amps. By extrapolation of a previous calibration graph of temperature (measured with an optical pyrometer) versus heating current, the temperature of the foil during oxidation was estimated to be in the region of 300°C . Subsequent to removal of the oxygen gas, the system was outgassed for 0.3 hours, with the foil still being maintained at -300°C so as to remove adsorbed oxygen, and finally for a further 2.0 hours at room temperature. Figure 1(c) is an auger spectrum of the oxidized strontium showing the expected large signal for lattice oxygen of SrO . However, it is further evident that the nickel peaks, at 716, 783, and 848 eV are also present, suggesting that during oxidation the strontium layer underwent some coalescence, thus forming crevices through which the nickel again became accessible to the scanning electron beam to some extent. The SAES spectrum shown in fig. 1(d) was taken after the final step in construction of the Ba/SrO/Ni system, viz. deposition of barium metal on top of the oxidised SrO layer. It shows the expected appearance of the characteristic Barium AES peaks and total attenuation of the nickel peaks once again. It is not clear whether the small oxygen peak originated from oxygen of

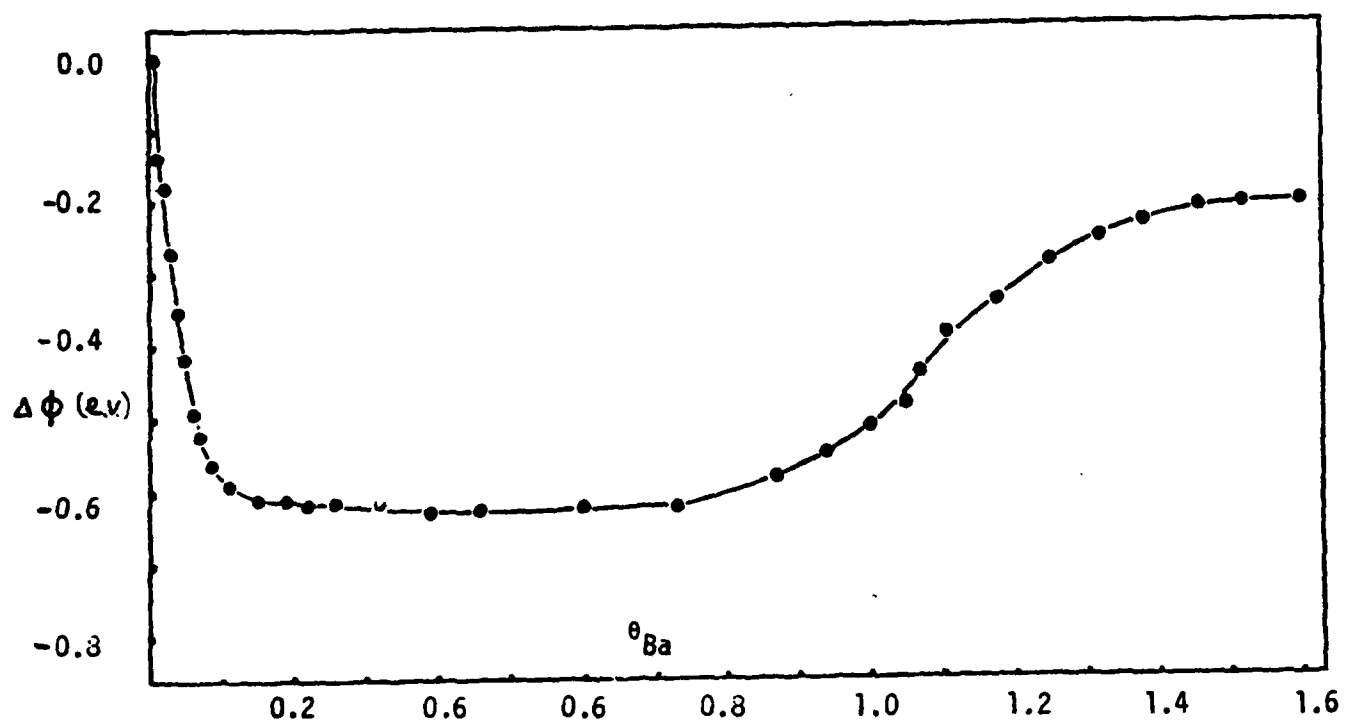


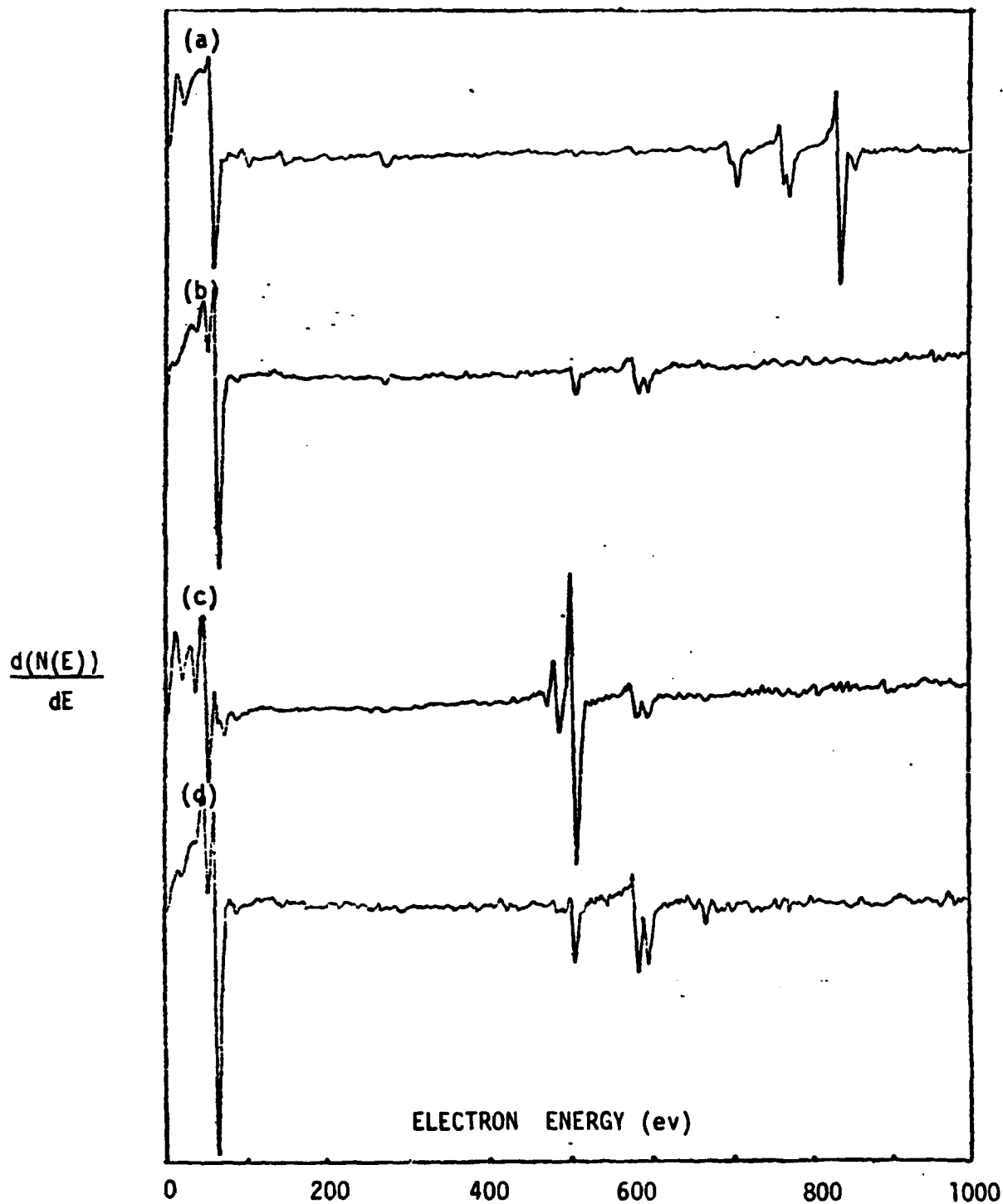
FIG-3 : Work function change ($\Delta\phi$) as a function of barium coverage (θ_{Ba}) on strontium oxide

the SrO layer or trace oxygen. Barium deposition on the SrO/Ni was made at a background pressure of 4×10^{-10} Torr and with heating current $I = 1.0$ A for the barium evaporator. The auger spectrum of the resultant Ba/SrO/Ni given in Figure 1(d) corresponds to a barium coverage of 1.7 monolayer, calculated on the basis of a "break-point" plot run under the same conditions, i.e. $I = 1.0$ A for the barium evaporator which gave a break-point-time of 58.4 minutes for a monolayer.

Figure 3 details the changes in work function observed during deposition of barium up to equivalence of 1.7 monolayers on top of the oxidised SrO layer. The rapid initial drop in work function caused by growth of the barium up to $\theta_{Ba} = 0.2$ monolayer is particularly noteworthy and appears fully consistent with the beneficial effects usually attributed to surface barium on oxide cathodes. The broad "valley" at low work function extending from $\theta_{Ba} = 0.2$ to $\theta_{Ba} = 0.7$ would also be beneficial in allowing ϕ to be independent of θ_{Ba} over this range. The rise in ϕ above approximately the equivalence of a monolayer of barium is comparable to results on other systems.

The Ba/BaO/Ni System:

In Figure 4(a) is given the auger spectrum of the nickel substrate. Figure 4(b) shows the auger spectrum after barium evaporation onto nickel initially with $I = 1.0$ A (evaporation time = 0.5 hours) and then with $I = 1.1$ A for a further 1.0 hours. The characteristic auger peaks of barium can be seen together with attenuation of the nickel. Although the background pressure was in the region of 6×10^{-10} Torr during evaporation; a small oxygen peak can be noted.



4 : Auger spectra of (a) nickel support after argon ion bombardment; (b) barium deposited at $P = 6.0 \times 10^{-10}$ Torr ($\theta_{Ba} = 4.5$); (c) barium oxidized at $P_0 = 5 \times 10^{-7}$ Torr at 300°C for 1.0 hours and outgassed at 300°C for 0.3 hours and (d) ^{238}Ba deposited on Ni/BaO ($\theta_{Ba} = 7.0$)

A break-point plot for barium evaporation at 1.1 A onto nickel was obtained in a separate experiment, as shown in Figure 5. This gave the break-point time for monolayer deposition as 15.0 minutes at 1.1 amps and implied that roughly 4.5 layers of barium had been deposited for the auger spectrum shown in Figure 4(b). This barium layer was then oxidized using the same procedure as used for strontium, the resulting auger spectrum of BaO/Ni being shown in Figure 4(c). The strong oxygen peak expected for lattice oxygen of BaO can be seen.

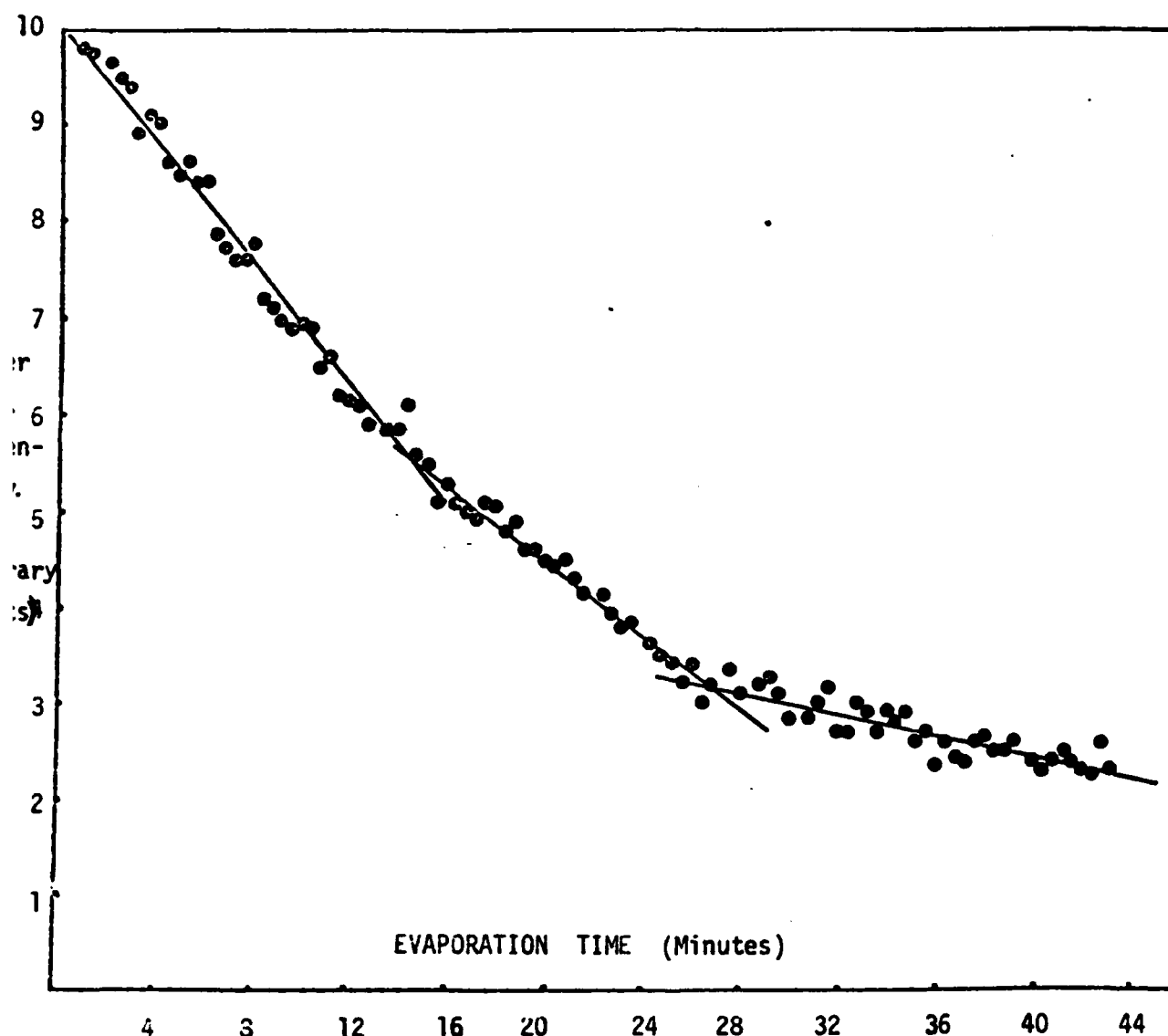


FIG. C-5: Intensity of the nickel auger peak as a function of barium evaporation time.

Evaporation of barium (I of the evaporator = 1.1 Å) onto the BaO layer allowed the Work Function (ϕ) vs. Coverage Curve shown in Figure 6 to be constructed. The final SAES spectrum shown in Figure 4(d) was taken after deposition of this barium overlayer on top of the oxidised BaO layer, and shows the expected enhancement of the Barium/Oxygen AES features.

Work function Values shown in Fig. 6 as a function of θ_{Ba} on BaO were calculated assuming a value of $\phi = 4.41$ e.V. for the nickel support. Despite the fact that identical procedures were adopted to measure ϕ in both systems the Ba/BaO/Ni case, unlike the Ba/SrO/Ni system, does not give a minimum in the plot of ϕ vs. θ_{Ba} , but an apparent maximum at $\theta_{Ba} \approx 0.25$. Figure 6 also shows that, for θ_{Ba} increasing upward from 0.25 at longer barium deposition times, the work function of the Ba/BaO/Ni system declined steadily. This appeared consistent with the idea that, for these larger depositions of barium, most Ba^0 remained on the surface thereby causing the effective work function to drop steadily towards the value for metallic barium. At nett depositions \geq ca. 7 monolayer equivalents the work function levelled off at ca. 2.4 eV which falls within the range of values in the literature for metallic barium (2.1 to 2.7 eV).

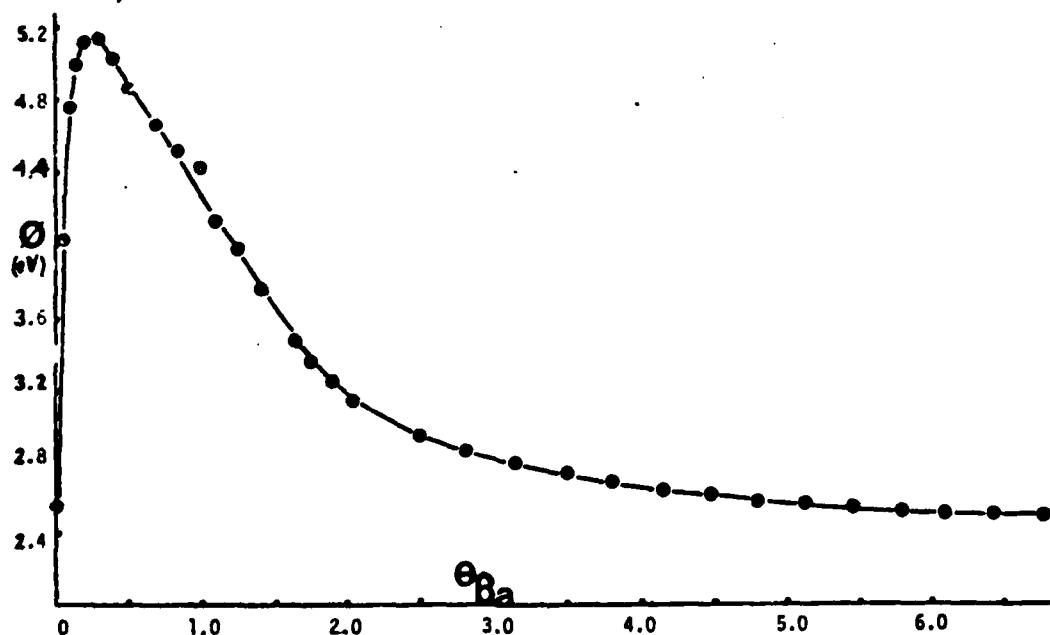


FIG. C-6: Variation in work function (ϕ) as a function of barium coverage (θ_{Ba}) on barium oxide.

END

FILMED

9-85

DTIC